8 LDA+DMFT: Linear Response Functions

Eva Pavarini
Institute for Advanced Simulation
Forschungszentrum Jülich

Contents

1 Introduction **2**

2 From DMFT to LDA+DMFT **4**
2.1 DMFT for a toy model: The Hubbard dimer 4
2.2 Non-local Coulomb interaction 11
2.3 Quantum-impurity solvers: Continuous-time quantum Monte Carlo 12
2.4 DMFT for the one-band Hubbard model 17
2.5 DMFT for multi-orbital models 20
2.6 LDA+DMFT: Model building 22

3 Linear response functions **26**
3.1 The generalized susceptibility 26
3.2 DMFT and Bethe-Salpeter equation 28
3.3 The local susceptibility: Legendre representation 31
3.4 Magnetic susceptibility for the single-band Hubbard model 32

4 Conclusion **38**

A Eigenstates of two-site models **39**
A.1 Hubbard dimer 39
A.2 Anderson molecule 41

B Lehmann representation of the local Green function **43**

C Atomic magnetic susceptibility **44**

E. Pavarini and E. Koch (eds.)
Topology, Entanglement, and Strong Correlations
Modeling and Simulation Vol. 10
Forschungszentrum Jülich, 2020, ISBN 978-3-95806-466-9
http://www.cond-mat.de/events/correl20

1 Introduction

The electronic many-body problem, in the non-relativistic limit and in the Born-Oppenheimer approximation, is described by the Hamiltonian

$$\hat{H}_e = -\frac{1}{2}\sum_i \nabla_i^2 - \sum_i \sum_\alpha \frac{Z_\alpha}{|\boldsymbol{r}_i - \boldsymbol{R}_\alpha|} + \sum_{i>j} \frac{1}{|\boldsymbol{r}_i - \boldsymbol{r}_j|} + \sum_{\alpha>\alpha'} \frac{Z_\alpha Z_{\alpha'}}{|\boldsymbol{R}_\alpha - \boldsymbol{R}_{\alpha'}|}, \tag{1}$$

where $\{\boldsymbol{r}_i\}$ are electron coordinates, $\{\boldsymbol{R}_\alpha\}$ nuclear coordinates and Z_α the nuclear charges. Using a complete one-electron basis, for example the basis $\{\phi_a(\boldsymbol{r})\}$, where $\{a\}$ are the quantum numbers, we can write this Hamiltonian in second quantization as

$$\hat{H}_e = \underbrace{-\sum_{ab} t_{ab} c_a^\dagger c_b}_{\hat{H}_0} + \underbrace{\frac{1}{2}\sum_{aa'bb'} U_{aa'bb'}\; c_a^\dagger c_{a'}^\dagger c_{b'} c_b}_{\hat{H}_U}.$$

Here the hopping integrals are given by

$$t_{ab} = -\int d\mathbf{r}\; \overline{\phi_a}(\boldsymbol{r}) \Big(-\frac{1}{2}\nabla^2 \underbrace{- \sum_\alpha \frac{Z_\alpha}{|\boldsymbol{r} - \boldsymbol{R}_\alpha|}}_{v_{\rm en}(\boldsymbol{r})} \Big) \phi_b(\boldsymbol{r}),$$

while the elements of the Coulomb tensor are

$$U_{aa'bb'} = \int d\mathbf{r}_2 \int d\mathbf{r}_2\; \overline{\phi_a}(\boldsymbol{r}_1)\, \overline{\phi_{a'}}(\boldsymbol{r}_2)\; \frac{1}{|\boldsymbol{r}_1 - \boldsymbol{r}_2|}\; \phi_{b'}(\boldsymbol{r}_2)\, \phi_b(\boldsymbol{r}_1).$$

In principle, all complete one-electron bases are equivalent. In practice, since, in the general case, we cannot solve the N-electron problem exactly, some bases are better than others. One possible choice for the basis are the Kohn-Sham orbitals, $\{\phi_a^{\rm KS}(\boldsymbol{r})\}$, obtained, e.g., in the local density approximation (LDA).[1] In this case, it is useful to replace the electron-nuclei interaction $v_{\rm en}(\boldsymbol{r})$ with the DFT potential $v_R(\boldsymbol{r})$, which includes in addition the Hartree term $v_{\rm H}(\boldsymbol{r})$ and the (approximate) exchange-correlation potential $v_{\rm xc}(\boldsymbol{r})$

$$v_{\rm R}(\boldsymbol{r}) = v_{\rm en}(\boldsymbol{r}) + \underbrace{\int d\mathbf{r}'\; \frac{n(\boldsymbol{r}')}{|\boldsymbol{r} - \boldsymbol{r}'|}}_{v_{\rm H}(\boldsymbol{r})} + v_{\rm xc}(\boldsymbol{r}),$$

so that

$$\tilde{t}_{ab} = -\int d\mathbf{r}\; \overline{\phi_a^{\rm KS}}(\boldsymbol{r}) \Big(-\frac{1}{2}\nabla^2 + v_{\rm R}(\boldsymbol{r}) \Big) \phi_b^{\rm KS}(\boldsymbol{r}). \tag{2}$$

To avoid double counting (DC), we have however to subtract from $\hat{H}_U$ the term $\hat{H}_{\rm DC}$, which describes the Coulomb terms already included in the hopping integrals

$$\hat{H}_e = \underbrace{-\sum_{ab} \tilde{t}_{ab}\, c_a^\dagger c_b}_{\hat{H}_0 = \hat{H}_e^{\rm LDA}} + \underbrace{\frac{1}{2}\sum_{aba'b'} \tilde{U}_{aa'bb'}\; c_a^\dagger c_{a'}^\dagger c_{b'} c_b - \hat{H}_{\rm DC}}_{\Delta \hat{H}_U}.$$

[1] For the purpose of many-body calculations the differences between LDA, GGA, or their plain extensions are in practice negligible; for simplicity, in the rest of the lecture, we thus adopt LDA as representative functional.

For weakly-correlated systems, in the Kohn-Sham basis, the effects included in $\Delta\hat{H}_U$ can, in first approximation, either be neglected or treated as a perturbation. This implies that $\hat{H}_e^{\rm LDA} \sim \hat{H}_{\rm eff}$, where $\hat{H}_{\rm eff}$ is the effective model which provides a good description of the system (at least) at low energy, and which describes emergent effective "elementary particles" and their interactions. Hypothetically, one could imagine that $\hat{H}_{\rm eff}$ is obtained via a canonical transformation, so that $\hat{H}_{\rm eff} \sim \hat{S}^{-1}\hat{H}_e\,\hat{S}$, although the exact form of the operator $\hat{S}$ is unknown.

A defining feature of strong-correlation effects is that they cannot be described via a single-electron Hamiltonian, however. A model of form $\hat{H}_e^{\rm LDA}$ does not capture the Mott metal-insulator transition, no matter what the specific values of the parameters $\tilde{t}_{ab}$ are.[2] Thus for strongly-correlated materials the low-energy effective model must have a different form. For Mott systems a canonical Hamiltonian is the Hubbard model

$$\hat{H} = -\sum_{\sigma}\sum_{ii'} t^{i,i'} c^{\dagger}_{i\sigma} c_{i'\sigma} + U\sum_{i} \hat{n}_{i\uparrow}\hat{n}_{i\downarrow}, \tag{3}$$

which includes, in addition to a single-electron term, the on-site Coulomb repulsion. This Hamiltonian captures the essence of the Mott transition. At half filling, for $U = 0$ it describes a paramagnetic metal, and for $t^{i,i'}(1-\delta_{i,i'})=0$ an insulating set of paramagnetic atoms. Unfortunately, differently from Hamiltonians of type $\hat{H}_e^{\rm LDA}$, Hubbard-like models cannot be solved exactly in the general case. Remarkably, till 30 years ago, no method for describing the complete phase diagram of (3) in one coherent framework, including the paramagnetic insulating phase, was actually known. This changed between 1989 and 1992, when the dynamical mean-field theory (DMFT) was developed [1–4]. The key idea of DMFT consists in mapping the Hubbard model onto a self-consistent *auxiliary quantum-impurity problem*, which can be solved exactly. The mapping is based on the *local dynamical self-energy approximation*, very good for realistic three-dimensional lattices—and becoming exact in the infinite coordination limit [1, 2].

DMFT was initially applied only to simple cases, due to limitations in model building, computational power, and numerical methods for solving the auxiliary impurity problem (the quantum-impurity solvers). In the last twenty years remarkable progress lifted many of these limitations. First, reliable schemes to build realistic low-energy materials-specific Hubbard-like models have been devised, in particular using Kohn-Sham localized Wannier functions. This is astonishing, given that we do not know the exact operator $\hat{S}$ which gives the effective low-energy Hamiltonian, and thus a truly systematic derivation is not possible. Second, key advances in quantum-impurity solvers and increasingly more powerful supercomputers made it possible to study always more complex many-body Hamiltonians. The approach which emerged, consisting in solving within DMFT materials-specific many-body Hamiltonians constructed via LDA, is known as the LDA+DMFT method [5–7]. This technique (and its extensions) is now the state-of-the-art for describing strongly-correlated materials. In this lecture I will outline the basic ideas on which the method is based, its successes and its limitations. This manuscripts extends the one of last year's school—in which more details on the model building aspects can be found—to the calculation of linear response functions.

[2] One can obtain an insulator by reducing the symmetry, e.g, by increasing the size of the primitive cell. This Slater-type insulator has however different properties than a Mott-type insulator.

2 From DMFT to LDA+DMFT

We will start by introducing the basics of DMFT. First we will consider a case for which analytic calculations can be performed, the two-site Hubbard Hamiltonian. This is a toy model, useful to illustrate how the method works, but for which, as we will see, DMFT is not a good approximation. Indeed, the Hubbard dimer is the worst case for DMFT, since the coordination number is the lowest possible. Next we will extend the formalism to the one-band and then to the multi-orbital Hubbard Hamiltonian. For three-dimensional lattices the coordination number is typically large and thus DMFT is an excellent approximation. Finally, we will discuss modern schemes to construct materials-specific many-body models. They are based on Kohn-Sham Wannier orbitals, calculated, e.g, using the LDA functional. The solution of such models via DMFT defines the LDA+DMFT method.

2.1 DMFT for a toy model: The Hubbard dimer

The two-site Hubbard model is given by

$$\hat{H} = \varepsilon_d \sum_{i\sigma} \hat{n}_{i\sigma} - t \sum_{\sigma} \left(c^\dagger_{1\sigma} c_{2\sigma} + c^\dagger_{2\sigma} c_{1\sigma} \right) + U \sum_i \hat{n}_{i\uparrow} \hat{n}_{i\downarrow},$$

with $i = 1, 2$. The ground state for $N = 2$ electrons (half filling) is the singlet[3]

$$|G\rangle_H = \frac{a_2(t,U)}{\sqrt{2}} \left(c^\dagger_{1\uparrow} c^\dagger_{2\downarrow} - c^\dagger_{1\downarrow} c^\dagger_{2\uparrow} \right) |0\rangle + \frac{a_1(t,U)}{\sqrt{2}} \left(c^\dagger_{1\uparrow} c^\dagger_{1\downarrow} + c^\dagger_{2\uparrow} c^\dagger_{2\downarrow} \right) |0\rangle \tag{4}$$

with

$$a_1^2(t,U) = \frac{1}{\Delta(t,U)} \frac{\Delta(t,U) - U}{2}, \qquad a_2^2(t,U) = \frac{4t^2}{\Delta(t,U)} \frac{2}{\Delta(t,U) - U},$$

and

$$\Delta(t,U) = \sqrt{U^2 + 16t^2}.$$

The energy of this state is

$$E_0(2) = 2\varepsilon_d + \frac{1}{2}\big(U - \Delta(t,U)\big).$$

In the $T \to 0$ limit, using the Lehmann representation (see Appendix B), one can show that the local Matsubara Green function for spin σ takes then the form

$$G^\sigma_{i,i}(i\nu_n) = \frac{1}{4} \Bigg(\frac{1 + w(t,U)}{i\nu_n - (E_0(2) - \varepsilon_d + t - \mu)} + \frac{1 - w(t,U)}{i\nu_n - \big(E_0(2) - \varepsilon_d - t - \mu\big)} + \frac{1 - w(t,U)}{i\nu_n - \big(-E_0(2) + U + 3\varepsilon_d + t - \mu\big)} + \frac{1 + w(t,U)}{i\nu_n - \big(-E_0(2) + U + 3\varepsilon_d - t - \mu\big)} \Bigg),$$

[3] Eigenstates and eigenvalues of the Hubbard dimer for arbitrary filling can be found in Appendix A.1.

where $\nu_n = \pi(2n+1)/\beta$ are fermionic Matsubara frequencies, $\mu = \varepsilon_d + U/2$ is the chemical potential, and the weight is $w(t,U) = 2a_1(t,U)a_2(t,U)$. The local Green function can be rewritten as the average of the Green function for the bonding ($k = 0$) and the anti-bonding state ($k = \pi$), i.e.,

$$G^\sigma_{i,i}(i\nu_n) = \frac{1}{2}\Bigg(\underbrace{\frac{1}{i\nu_n + \mu - \varepsilon_d + t - \Sigma^\sigma(0,i\nu_n)}}_{G^\sigma(0,i\nu_n)} + \underbrace{\frac{1}{i\nu_n + \mu - \varepsilon_d - t - \Sigma^\sigma(\pi,i\nu_n)}}_{G^\sigma(\pi,i\nu_n)} \Bigg).$$

The self-energy is given by

$$\Sigma^\sigma(k,i\nu_n) = \frac{U}{2} + \frac{U^2}{4}\frac{1}{i\nu_n + \mu - \varepsilon_d - \frac{U}{2} - \ e^{ik}\ 3t}.$$

The self-energies $\Sigma^\sigma(0,i\nu_n)$ and $\Sigma^\sigma(\pi,i\nu_n)$ differ due to the phase $e^{ik} = \pm 1$ in their denominators. The local self-energy is, by definition, the average of the two

$$\Sigma^\sigma_l(i\nu_n) = \frac{1}{2}\Big(\Sigma^\sigma(\pi,i\nu_n) + \Sigma^\sigma(0,i\nu_n) \Big) = \frac{U}{2} + \frac{U^2}{4}\ \frac{i\nu_n + \mu - \varepsilon_d - \frac{U}{2}}{(i\nu_n + \mu - \varepsilon_d - \frac{U}{2})^2 - (3t)^2}.$$

The difference

$$\Delta\Sigma^\sigma_l(i\nu_n) = \frac{1}{2}\Big(\Sigma^\sigma(\pi,i\nu_n) - \Sigma^\sigma(0,i\nu_n) \Big) = \frac{U^2}{4}\ \frac{3t}{(i\nu_n + \mu - \varepsilon_d - \frac{U}{2})^2 - (3t)^2},$$

thus measures the importance of non-local effects; it would be zero if the self-energy was independent of $\boldsymbol{k}$. Next we define the hybridization function

$$F^\sigma(i\nu_n) = \frac{\big(t + \Delta\Sigma^\sigma_l(i\nu_n)\big)^2}{i\nu_n + \mu - \varepsilon_d - \Sigma^\sigma_l(i\nu_n)}$$

which for $U = 0$ becomes

$$F^\sigma_0(i\nu_n) = \frac{t^2}{i\nu_n}.$$

By using these definitions, we can rewrite the local Green function as

$$G^\sigma_{i,i}(i\nu_n) = \frac{1}{i\nu_n + \mu - \varepsilon_d - F^\sigma(i\nu_n) - \Sigma^\sigma_l(i\nu_n)}. \tag{5}$$

It is important to point out that, as one may see from the formulas above, the local Green function and the local self-energy satisfy the following *local Dyson equation*

$$\Sigma^\sigma_l(i\nu_n) = \frac{1}{\mathfrak{G}^\sigma_{i,i}(i\nu_n)} - \frac{1}{G^\sigma_{i,i}(i\nu_n)},$$

where $\mathfrak{G}^\sigma_{i,i}(i\nu_n)$ is given by

$$\mathfrak{G}^\sigma_{i,i}(i\nu_n) = \frac{1}{i\nu_n + \mu - \varepsilon_d - F^\sigma(i\nu_n)}.$$

Thus, one could think of mapping the Hubbard dimer into an auxiliary quantum-impurity model, chosen such that, within certain approximations, the impurity Green function is as close as possible to the local Green function of the original problem. How can we do this? Let us adopt as auxiliary model the Anderson molecule

$$\hat{H}^{\rm A} = \varepsilon_s \sum_\sigma \hat{n}_{s\sigma} - t \sum_\sigma \left(c^\dagger_{d\sigma} c_{s\sigma} + c^\dagger_{s\sigma} c_{d\sigma} \right) + \varepsilon_d \sum_\sigma \hat{n}_{d\sigma} + U \hat{n}_{d\uparrow} \hat{n}_{d\downarrow}. \tag{6}$$

The first constraint would be that Hamiltonian (6) has a ground state with the same occupations of the 2-site Hubbard model, i.e., at half filling, $n_d = n_s = 1$. Such a *self-consistency condition* is satisfied if $\varepsilon_s = \mu = \varepsilon_d + U/2$. This can be understood by comparing the Hamiltonian matrices of the two models in the Hilbert space with $N = 2$ electrons. To this end, we first order the two-electron states of the Hubbard dimer as

$$|1\rangle = c^\dagger_{1\uparrow} c^\dagger_{2\uparrow} |0\rangle, \qquad |4\rangle = \tfrac{1}{\sqrt{2}} (c^\dagger_{1\uparrow} c^\dagger_{2\downarrow} - c^\dagger_{1\downarrow} c^\dagger_{2\uparrow}) |0\rangle,$$

$$|2\rangle = c^\dagger_{1\downarrow} c^\dagger_{2\downarrow} |0\rangle, \qquad |5\rangle = c^\dagger_{1\uparrow} c^\dagger_{1\downarrow} |0\rangle,$$

$$|3\rangle = \tfrac{1}{\sqrt{2}} (c^\dagger_{1\uparrow} c^\dagger_{2\downarrow} + c^\dagger_{1\downarrow} c^\dagger_{2\uparrow}) |0\rangle, \qquad |6\rangle = c^\dagger_{2\uparrow} c^\dagger_{2\downarrow} |0\rangle.$$

In this basis the Hamiltonian of the Hubbard dimer has the matrix form

$$\hat{H}_2(\varepsilon_d, U, t) = \begin{pmatrix} 2\varepsilon_d & 0 & 0 & 0 & 0 & 0 \\ 0 & 2\varepsilon_d & 0 & 0 & 0 & 0 \\ 0 & 0 & 2\varepsilon_d & 0 & 0 & 0 \\ 0 & 0 & 0 & 2\varepsilon_d & -\sqrt{2}t & -\sqrt{2}t \\ 0 & 0 & 0 & -\sqrt{2}t & 2\varepsilon_d{+}U & 0 \\ 0 & 0 & 0 & -\sqrt{2}t & 0 & 2\varepsilon_d{+}U \end{pmatrix}.$$

The ground state, the singlet given in Eq. (4), can be obtained by diagonalizing the lower $3{\times}3$ block. For the Anderson molecule, ordering the basis in the same way ($1 \to d, 2 \to s$), this Hamiltonian becomes

$$\hat{H}^A_2(\varepsilon_d, U, t; \varepsilon_s) = \begin{pmatrix} \varepsilon_d{+}\varepsilon_s & 0 & 0 & 0 & 0 & 0 \\ 0 & \varepsilon_d{+}\varepsilon_s & 0 & 0 & 0 & 0 \\ 0 & 0 & \varepsilon_d{+}\varepsilon_s & 0 & 0 & 0 \\ 0 & 0 & 0 & \varepsilon_d{+}\varepsilon_s & -\sqrt{2}t & -\sqrt{2}t \\ 0 & 0 & 0 & -\sqrt{2}t & 2\varepsilon_d{+}U & 0 \\ 0 & 0 & 0 & -\sqrt{2}t & 0 & 2\varepsilon_s \end{pmatrix}.$$

Comparing the lower $3{\times}3$ block of $\hat{H}^A_2(\varepsilon_d, U, t; \varepsilon_s)$ with the corresponding block of $\hat{H}_2(\varepsilon_d, U, t)$ we can see that, unless $\varepsilon_s = \mu = \varepsilon_d + U/2$, the two ionic states $|5\rangle$ and $|6\rangle$ have different energies; hence, for $\varepsilon_s \neq \mu$, the two sites are differently occupied in the ground state.

By setting $\varepsilon_s = \mu$ we find that $\hat{H}_2^A(\varepsilon_d, U, t; \mu) = \hat{H}_2(\varepsilon_d + \frac{U}{4}, \frac{U}{2}, t)$. The $N = 2$ ground state of $\hat{H}_2^A(\varepsilon_d, U, t; \mu)$ has thus the form of the ground-state for the Hubbard dimer

$$|G\rangle_A = \frac{a_2(t, U/2)}{\sqrt{2}} \left(c_{d\uparrow}^\dagger c_{s\downarrow}^\dagger - c_{d\downarrow}^\dagger c_{s\uparrow}^\dagger \right) |0\rangle + \frac{a_1(t, U/2)}{\sqrt{2}} \left(c_{d\uparrow}^\dagger c_{d\downarrow}^\dagger + c_{s\uparrow}^\dagger c_{s\downarrow}^\dagger \right) |0\rangle,$$

and the condition $n_s = n_d = 1$ is satisfied. Since $\varepsilon_s \neq \varepsilon_d$, however, the eigenstates of $\hat{H}^{\mathrm{A}}$ for one electron ($N = 1$) or one hole ($N = 3$) are not the bonding and antibonding states.[4] The impurity Green function is then given by

$$G_{d,d}^\sigma(i\nu_n) = \frac{1}{4} \Bigg(\frac{1 + w'(t,U)}{i\nu_n - (E_0(2) - E_-(1) - \mu)} + \frac{1 - w'(t,U)}{i\nu_n - (E_0(2) - E_+(1) - \mu)} \\ \frac{1 + w'(t,U)}{i\nu_n - (E_-(3) - E_0(2) - \mu)} + \frac{1 - w'(t,U)}{i\nu_n - (E_+(3) - E_0(2) - \mu)} \Bigg),$$

where

$$E_0(2) - E_\pm(1) - \mu = -\Big(E_\pm(3) - E_0(2) - \mu \Big) = -\frac{1}{4} \Big(2\Delta(t, U/2) \pm \Delta(t, U) \Big),$$

and

$$w'(t, U) = \frac{1}{2} \frac{32t^2 - U^2}{\Delta(t, U)\Delta(t, U/2)}.$$

After some rearrangement we obtain a much simpler expression

$$G_{d,d}^\sigma(i\nu_n) = \frac{1}{i\nu_n + \mu - \varepsilon_d - \mathcal{F}_0^\sigma(i\nu_n) - \Sigma_A^\sigma(i\nu_n)}.$$

The impurity self-energy equals the local self-energy of the Hubbard dimer

$$\Sigma_A^\sigma(i\nu_n) = \frac{U}{2} + \frac{U^2}{4} \frac{i\nu_n}{(i\nu_n)^2 - (3t)^2}.$$

The hybridization function is given by

$$\mathcal{F}_0^\sigma(i\nu_n) = \frac{t^2}{i\nu_n}.$$

For $U = 0$, $G_{d,d}^\sigma(i\nu_n)$ equals the non-interacting impurity Green function

$$G_{d,d}^{0\sigma}(i\nu_n) = \frac{1}{i\nu_n + \mu - \varepsilon_d - \mathcal{F}_0^\sigma(i\nu_n)}.$$

The impurity Green function thus satisfies the *impurity Dyson equation*

$$\Sigma_A^\sigma(i\nu_n) = \frac{1}{G_{d,d}^{0\sigma}(i\nu_n)} - \frac{1}{G_{d,d}^\sigma(i\nu_n)}.$$

[4] The complete list of eigenvalues and eigenvectors of the Anderson molecule for $\varepsilon_s = \varepsilon_d + U/2$ and arbitrary electron number N can be found in Appendix A.2.

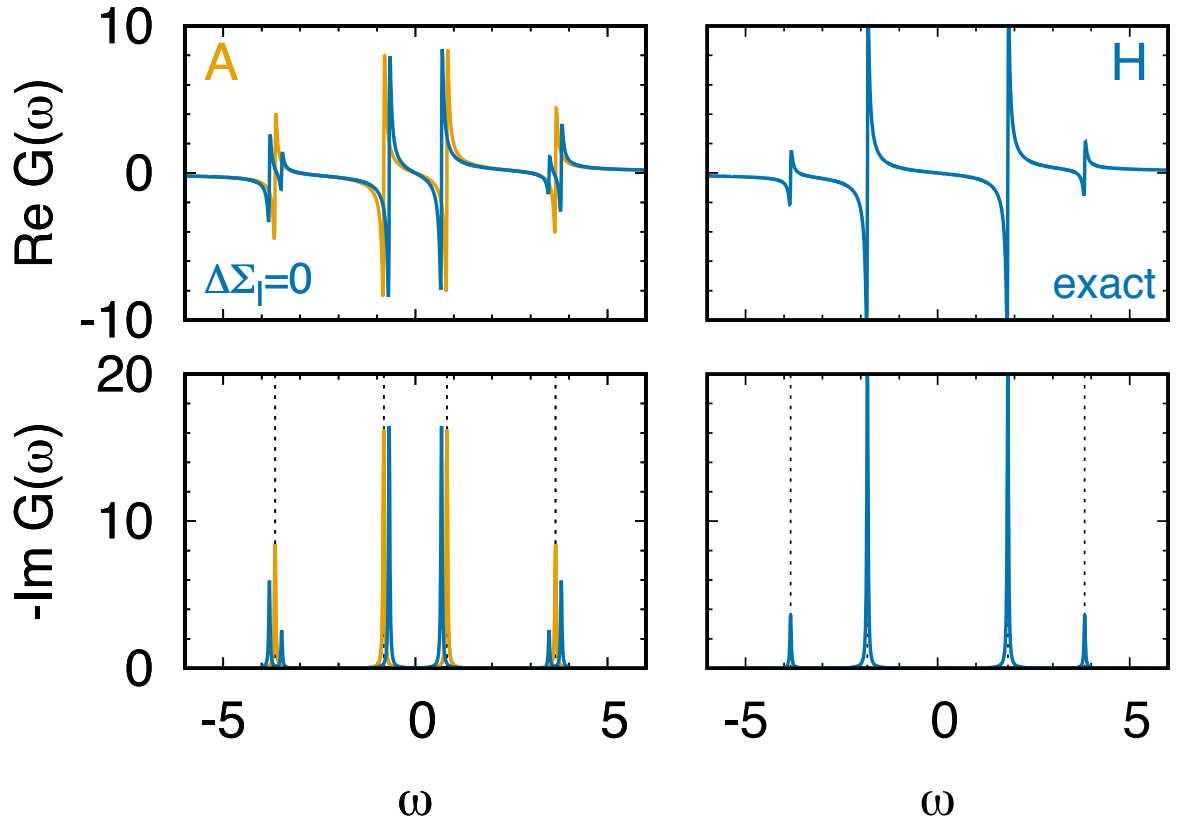

Fig. 1: *Green functions of the Hubbard dimer ($t = 1, U = 4$) and the Anderson molecule ($\varepsilon_s = \varepsilon_d + U/2$) in the zero temperature limit. Left panels, blue: Hubbard dimer with local self-energy only, i.e., with $\Delta\Sigma_l^\sigma(\omega) = 0$. Left panels, orange: Anderson molecule. Right panels: Exact Green function of the Hubbard dimer. Dashed lines: Poles of the Green function of the Anderson molecule (left) or Hubbard dimer (right).*

In Fig. 1 we show the impurity Green function of the Anderson molecule (orange, left panels) and the local Green function of the 2-site Hubbard model, in the local self-energy approximation (blue, left panels) and exact (blue, right panels). Comparing left and right panels we can see that setting $\Delta\Sigma_l^\sigma(\omega) = 0$ yields large errors. The left panels demonstrate, however, that the spectral function of the Anderson molecule is quite similar to the one of the Hubbard dimer with $\Delta\Sigma_l^\sigma(\omega) = 0$. The small remaining deviations come from the fact that, for the Hubbard dimer, in the impurity Dyson equation, the non-interacting impurity Green function is replaced by $\mathfrak{G}_{i,i}^\sigma(i\nu_n)$ in the local self-energy approximation, i.e., with the *bath* Green function

$$\mathcal{G}_{i,i}^\sigma(i\nu_n) = \frac{1}{i\nu_n + \mu - \varepsilon_d - \mathcal{F}_l^\sigma(i\nu_n)},$$

where

$$\mathcal{F}_l^\sigma(i\nu_n) = \frac{t^2}{i\nu_n + \mu - \varepsilon_d - \Sigma_A^\sigma(i\nu_n)}.$$

We are now in the position of explaining how DMFT works for the Hamiltonian of the Hubbard dimer, choosing the Anderson molecule Hamiltonian (6) as the auxiliary quantum-impurity model. The procedure can be split in the following steps

1. Build the initial quantum-impurity model with $G^{0\sigma}_{d,d}(i\nu_n) = G^{0\sigma}_{i,i}(i\nu_n)$. The initial bath is thus defined by energy $\varepsilon_s = \varepsilon_d$ and hopping t.

2. Calculate the local Green function $G^{\sigma}_{d,d}(i\nu_n)$ for the auxiliary model.

3. Use the local Dyson equation to calculate the impurity self-energy

$$\Sigma^{\sigma}_{A}(i\nu_n) = \frac{1}{G^{0\sigma}_{d,d}(i\nu_n)} - \frac{1}{G^{\sigma}_{d,d}(i\nu_n)}.$$

4. Calculate the local Green function of the Hubbard dimer setting the self-energy equal to the one of the quantum-impurity model

$$G^{\sigma}_{i,i}(i\nu_n) \sim \frac{1}{2}\left(\frac{1}{i\nu_n + \mu - \varepsilon_d + t - \Sigma^{\sigma}_{A}(i\nu_n)} + \frac{1}{i\nu_n + \mu - \varepsilon_d - t - \Sigma^{\sigma}_{A}(i\nu_n)}\right).$$

5. Calculate a new bath Green function $\mathcal{G}^{\sigma}_{i,i}(i\nu_n)$ from the local Dyson equation

$$\mathcal{G}^{\sigma}_{i,i}(i\nu_n) = \frac{1}{\Sigma^{\sigma}_{A}(i\nu_n) + 1/G^{\sigma}_{i,i}(i\nu_n)}.$$

6. Build a new $G^{0\sigma}_{d,d}(i\nu_n)$ from $\mathcal{G}^{\sigma}_{i,i}(i\nu_n)$.

7. Restart from the second step.

8. Iterate till self-consistency, i.e., here till $n^{\sigma}_{d} = n^{\sigma}_{i}$ and $\Sigma^{\sigma}_{A}(i\nu_n)$ does not change any more.

The Anderson molecule satisfies the self-consistency requirements for $\varepsilon_s = \mu$. The remaining difference between $G^{\sigma}_{d,d}(i\nu_n)$, the impurity Green function, and $G^{\sigma}_{i,i}(i\nu_n)$, the local Green function of the Hubbard dimer in the local self-energy approximation, arises from the difference in the associated hybridization functions

$$\Delta\mathcal{F}_l(i\nu_n) = \mathcal{F}^{\sigma}_{l}(i\nu_n) - \mathcal{F}^{\sigma}_{0}(i\nu_n) = t^2p^2\left(-\frac{2}{i\nu_n} + \frac{1}{i\nu_n - \varepsilon_a} + \frac{1}{i\nu_n + \varepsilon_a}\right)$$

where $p^2 = U^2/8\varepsilon_a^2$ and $\varepsilon_a = \sqrt{9t^2 + U^2/4}$. If we use the Anderson molecule as quantum-impurity model we neglect $\Delta\mathcal{F}_l(i\nu_n)$; the error made is small, as shown in the left panels of Fig. 1. To further improve we would have to modify the auxiliary model adding more bath sites. Remaining with the Anderson molecule, let us compare in more detail its spectral function with the exact spectral function of the Hubbard dimer. Fig. 2 shows that the evolution as a function of U is different for the two Hamiltonians. Anticipating the discussion of later sections, if we compare to the spectral function of the actual lattice Hubbard model, we could say that the Anderson molecule partially captures the behavior of the central "quasi-particle" or "Kondo"

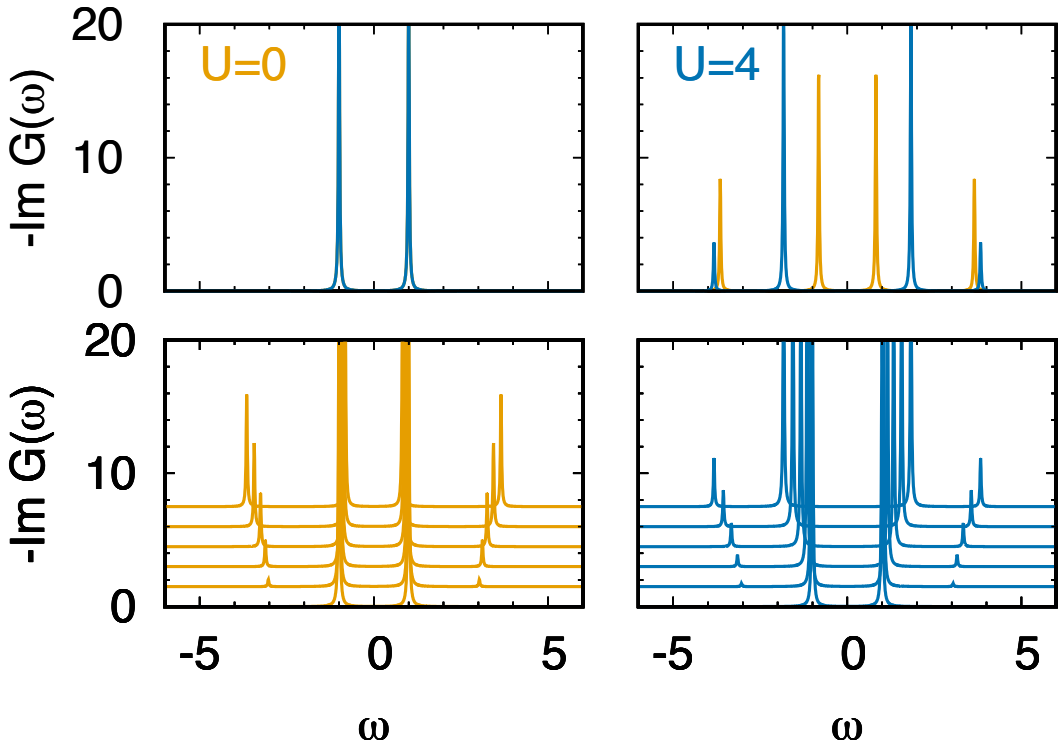

Fig. 2: *Imaginary part of the Green function of the Anderson molecule (orange) and Hubbard dimer (blue) in the zero temperature limit. For the Hubbard dimer the exact Green functions are used, as in the right panels of Fig. 1. Parameters:* $t = 1$, $\varepsilon_s = \mu$. *Top:* $U = 0$ *(left) and* $U = 4t$ *(right). Bottom: Evolution with increasing* U *from* 0 *to* $4t$ *in equal steps.*

peak with increasing U, although the Kondo effect itself is unrealistically described; as a matter of fact, the Kondo energy gain (the "Kondo temperature") is perturbative ($\propto t^2/U$) in the case of the Anderson molecule, while it is exponentially small for a Kondo impurity in a metallic bath. On the other hand, the Hubbard dimer captures well the Hubbard bands and the gap in the large-U limit. The example of the Anderson molecule also points to the possible shortcomings of DMFT calculations for the lattice Hubbard model (3) in which the quantum-impurity model is solved via exact diagonalization, however using a single bath site or very few; this might perhaps be sufficient in the limit of large gap,[5] but is bound to eventually fail approaching the metallic regime. Indeed, this failure is one of the reasons why the solution of the Kondo problem required the development of—at the time new—non-perturbative techniques such as the numerical renormalization group. Finally, the example of the Hubbard dimer shows that DMFT is not a good approximation for molecular complexes with two (or few) correlated sites. This is because in such systems the coordination number is the lowest possible, the worst case for dynamical mean-field theory. In three dimensional crystals, instead, the coordination number is typically large enough to make DMFT an excellent approximation.

[5]For a discussion of bath parametrization in exact diagonalization and the actual convergence with the number of bath sites for the lattice Hubbard model see Ref. [8].

2.2 Non-local Coulomb interaction

In Sec. 2.1 we have seen that the local Coulomb interaction gives rise, *alone*, to non-local self-energy terms, which can be very important. What is, instead, the effect of the non-local part of the Coulomb interaction? For a Hubbard dimer, extending the Coulomb interaction to first neighbors leads to the Hamiltonian

$$\begin{aligned}\hat{H} =&\varepsilon_d \sum_{i\sigma} \hat{n}_{i\sigma} - t \sum_{\sigma} \left(c^\dagger_{1\sigma} c_{2\sigma} + c^\dagger_{2\sigma} c_{1\sigma} \right) + U \sum_{i=1,2} \hat{n}_{i\uparrow} \hat{n}_{i\downarrow} \\ &+ \sum_{\sigma\sigma'} \left(V - 2J_V - J_V\, \delta_{\sigma\sigma'} \right) \hat{n}_{1\sigma} \hat{n}_{2\sigma'} - J_V \sum_{i\neq i'} \left(c^\dagger_{i\uparrow} c_{i\downarrow} c^\dagger_{i'\downarrow} c_{i'\uparrow} + c^\dagger_{i'\uparrow} c^\dagger_{i'\downarrow} c_{i\uparrow} c_{i\downarrow} \right),\end{aligned}$$

where the parameters in the last two terms are the intersite direct (V) and exchange (J_V) Coulomb interaction. For two electrons the Hamiltonian, in a matrix form, becomes

$$\hat{H}_2^{\mathrm{NL}} = \begin{pmatrix} 2\varepsilon_d{+}V{-}3J_V & 0 & 0 & 0 & 0 & 0 \\ 0 & 2\varepsilon_d{+}V{-}3J_V & 0 & 0 & 0 & 0 \\ 0 & 0 & 2\varepsilon_d{+}V{-}3J_V & 0 & 0 & 0 \\ 0 & 0 & 0 & 2\varepsilon_d{+}V{-}J_V & -\sqrt{2}t & -\sqrt{2}t \\ 0 & 0 & 0 & -\sqrt{2}t & 2\varepsilon_d{+}U & -J_V \\ 0 & 0 & 0 & -\sqrt{2}t & -J_V & 2\varepsilon_d{+}U \end{pmatrix}.$$

Since $J_V > 0$, the effect of J_V is to lower the energy of triplet states with respect singlet states. This might change the nature of the ground state. If, however, J_V is sufficiently small, the ground state remains a singlet. Setting for simplicity $J_V = 0$, we can notice that $\hat{H}_2^{\mathrm{NL}}$ equals $\hat{H}_2(\varepsilon'_d, U', t)$, the corresponding $N{=}2$-electron Hamiltonian of the $J_V{=}V{=}0$ Hubbard dimer, with parameters $\varepsilon'_d = \varepsilon_d + V/2$ and $U'{=}U{-}V$. The $N{=}2$ ground state is thus still given by Eq. (4), provided, however, that we replace U with U' in the coefficients. Eventually, in the limiting case $U{=}V$, $\hat{H}_2^{\mathrm{NL}}$ equals the corresponding Hamiltonian of an effective non-correlated dimer. What happens away from half filling? For $N{=}1$ electrons, eigenvectors and eigenvalues are the same as in the $V{=}0$ case; for $N{=}3$ electrons all energies are shifted by $2V$. This leads to further differences in the local Green function with respect to the $V{=}0$ case—in addition to those arising from replacing U with U'; to some extent, these additional changes can be interpreted as a hopping enhancement from t to $t + V/2$. Putting all these results together, we could thus say that, in first approximation, the (positive) intersite coupling V effectively reduces the strength of correlations.

In conclusion, *strong-correlation* effects typically appear when the *local term of the electron-electron repulsion dominates*, i.e., when it is much larger than long-range terms. Instead, a hypothetical system in which the Coulomb interaction strength is independent on the distance between sites (here $U{=}V$) is likely to be already well described via an *effective weakly correlated model*. Of course, in real materials, the effects of long-range Coulomb repulsion can be much more complicated than in the two-site model just discussed, but the general considerations made here remain true even in realistic cases.

2.3 Quantum-impurity solvers: Continuous-time quantum Monte Carlo

For the case of the Anderson molecule exact diagonalization is the simplest quantum-impurity solver and the one that provides most insights. Methods based on quantum Monte Carlo (QMC) sampling are often, however, the only option for realistic multi-orbital and/or multi-site models. Here we explain how to obtain the impurity Green function of the Anderson molecule via hybridization-expansion continuous-time QMC [9], a very successful QMC-based quantum-impurity solver. In this approach, the first step consists in splitting the Hamiltonian into bath ($\hat{H}_{\rm bath}$), hybridization ($\hat{H}_{\rm hyb}$), and local ($\hat{H}_{\rm loc}$) terms

$$\hat{H}^{\rm A} = \underbrace{\varepsilon_s \sum_\sigma \hat{n}_{s\sigma}}_{\hat{H}_{\rm bath}} \underbrace{-t \sum_\sigma \left(c^\dagger_{d\sigma} c_{s\sigma} + c^\dagger_{s\sigma} c_{d\sigma} \right)}_{\hat{H}_{\rm hyb}} + \underbrace{\varepsilon_d \sum_\sigma \hat{n}_{d\sigma} + U \hat{n}_{d\uparrow} \hat{n}_{d\downarrow}}_{\hat{H}_{\rm loc}} .$$

Next, we write the partition function Z as a perturbation series in the hybridization. To this end, we define $\hat{H}_0 = \hat{H}_{\rm bath} + \hat{H}_{\rm loc}$ and rewrite the partition function as

$$Z = {\rm Tr} \left(e^{-\beta(\hat{H}_0 - \mu \hat{N})} \hat{V}(\beta) \right)$$

where the operator $\hat{V}(\beta)$ is given by

$$\hat{V}(\beta) = e^{\beta(\hat{H}_0 - \mu\hat{N})} e^{-\beta(\hat{H}_0 + \hat{H}_{\rm hyb} - \mu\hat{N})} = \sum_m \underbrace{\int_0^\beta d\tau_1 \cdots \int_{\tau_{m-1}}^\beta d\tau_m}_{\int d\boldsymbol{\tau}^m} \underbrace{(-1)^m \prod_{l=m}^1 \hat{H}_{\rm hyb}(\tau_l)}_{\hat{O}^m(\boldsymbol{\tau})},$$

and

$$\hat{H}_{\rm hyb}(\tau_l) = e^{\tau_l(\hat{H}_0 - \mu\hat{N})} \hat{H}_{\rm hyb} e^{-\tau_l(\hat{H}_0 - \mu\hat{N})} = -t \sum_\sigma \left(c^\dagger_{d\sigma_l}(\tau_l) c_{s\sigma_l}(\tau_l) + c^\dagger_{s\sigma_l}(\tau_l) c_{d\sigma_l}(\tau_l) \right).$$

In this expansion, the only terms that contribute to the trace are even order ones ($m = 2k$) and they are products of impurity (d) and bath (s) creator-annihilator pairs. We can thus rewrite

$$\int d\boldsymbol{\tau}^{2k} \longrightarrow \int d\boldsymbol{\tau}^k \int d\bar{\boldsymbol{\tau}}^k \qquad\qquad \hat{O}^{2k}(\boldsymbol{\tau}) \longrightarrow \sum_{\boldsymbol{\sigma},\bar{\boldsymbol{\sigma}}} \hat{O}^{2k}_{\boldsymbol{\sigma},\bar{\boldsymbol{\sigma}}}(\boldsymbol{\tau}, \bar{\boldsymbol{\tau}})$$

where

$$\hat{O}^{2k}_{\boldsymbol{\sigma},\bar{\boldsymbol{\sigma}}}(\boldsymbol{\tau}, \bar{\boldsymbol{\tau}}) = (t)^{2k} \prod_{i=1}^k \left(c^\dagger_{d\bar{\sigma}_i}(\bar{\tau}_i) c_{s\bar{\sigma}_i}(\bar{\tau}_i) c^\dagger_{s\sigma_i}(\tau_i) c_{d\sigma_i}(\tau_i) \right).$$

The vector $\boldsymbol{\sigma} = (\sigma_1, \sigma_2, ..., \sigma_k)$ gives the spins $\{\sigma_i\}$ associated with the k impurity annihilators at imaginary times $\{\tau_i\}$, while $\bar{\boldsymbol{\sigma}} = (\bar{\sigma}_1, \bar{\sigma}_2, ..., \bar{\sigma}_k)$ gives the spins $\{\bar{\sigma}_i\}$ associated with the k impurity creators at imaginary times $\{\bar{\tau}_i\}$. It follows that the local and bath traces can be

decoupled and the partition function can be rewritten as

$$\frac{Z}{Z_{\rm bath}} = \sum_k \int^k d\boldsymbol{\tau} \int^k d\bar{\boldsymbol{\tau}} \sum_{\boldsymbol{\sigma},\bar{\boldsymbol{\sigma}}} d^k_{\bar{\boldsymbol{\sigma}},\boldsymbol{\sigma}}(\boldsymbol{\tau},\bar{\boldsymbol{\tau}}) t^k_{\boldsymbol{\sigma},\bar{\boldsymbol{\sigma}}}(\boldsymbol{\tau},\bar{\boldsymbol{\tau}})$$

$$d^k_{\bar{\boldsymbol{\sigma}},\boldsymbol{\sigma}}(\boldsymbol{\tau},\bar{\boldsymbol{\tau}}) = (t)^{2k}\ {\rm Tr}_{\rm bath}\left(e^{-\beta(\hat{H}_{\rm bath}-\mu\hat{N}_s)}\mathcal{T}\Pi^1_{i=k} c^\dagger_{s\sigma_i}(\tau_i) c_{s\bar{\sigma}_i}(\bar{\tau}_i)\right)/Z_{\rm bath}$$

$$t^k_{\boldsymbol{\sigma},\bar{\boldsymbol{\sigma}}}(\boldsymbol{\tau},\bar{\boldsymbol{\tau}}) = {\rm Tr}_{\rm loc}\left(e^{-\beta(\hat{H}_{\rm loc}-\mu\hat{N}_d)}\mathcal{T}\Pi^1_{i=k} c_{d\sigma_i}(\tau_i) c^\dagger_{d\bar{\sigma}_i}(\bar{\tau}_i)\right),$$

where $Z_{\rm bath} = 1 + 2e^{-\beta(\varepsilon_s-\mu)} + e^{-2\beta(\varepsilon_s-\mu)}$ and

$$c_{d\sigma}(\tau) = e^{\tau(\hat{H}_{\rm loc}-\mu\hat{N}_d)} c_{d\sigma} e^{-\tau(\hat{H}_{\rm loc}-\mu\hat{N}_d)}, \qquad c_{s\sigma}(\tau) = e^{\tau(\hat{H}_{\rm bath}-\mu\hat{N}_s)} c_{s\sigma} e^{-\tau(\hat{H}_{\rm bath}-\mu\hat{N}_s)}.$$

The trace involving only bath operators is simple to calculate, since $\hat{H}_{\rm bath}$ describes an independent-electron problem, for which Wick's theorem holds. It is given by the determinant

$$d^k_{\bar{\boldsymbol{\sigma}},\boldsymbol{\sigma}}(\boldsymbol{\tau},\bar{\boldsymbol{\tau}}) = \det\left(\mathcal{F}^k_{\bar{\boldsymbol{\sigma}},\boldsymbol{\sigma}}(\boldsymbol{\tau},\bar{\boldsymbol{\tau}})\right)$$

of the $k\times k$ non-interacting hybridization-function matrix, with elements

$$\left(\mathcal{F}^k_{\bar{\boldsymbol{\sigma}},\boldsymbol{\sigma}}(\boldsymbol{\tau},\bar{\boldsymbol{\tau}})\right)_{i',i} = \mathcal{F}^0_{\bar{\sigma}_{i'},\sigma_i}(\bar{\tau}_{i'}-\tau_i)$$

where

$$\mathcal{F}^0_{\bar{\sigma},\sigma}(\tau) = \delta_{\bar{\sigma},\sigma}\frac{t^2}{1+e^{-\beta(\varepsilon_s-\mu)}} \times \begin{cases} -e^{-\tau(\varepsilon_s-\mu)} & \tau > 0, \\ +e^{-(\beta+\tau)(\varepsilon_s-\mu)} & \tau < 0. \end{cases}$$

This is the imaginary time Fourier transform of the hybridization function introduced previously

$$\mathcal{F}^0_{\bar{\sigma},\sigma}(i\nu_n) = \frac{t^2}{i\nu_n - (\varepsilon_s-\mu)}\,\delta_{\bar{\sigma},\sigma}.$$

The calculation of the local trace is in general more complicated. In the case discussed here, the Hamiltonian does not flip spins. Thus only terms with an equal number of creation and annihilation operators *per spin* contribute to the local trace, and we can express the partition function in expansion orders per spin, k_σ. This yields [10]

$$\frac{Z}{Z_{\rm bath}} = \left(\prod_\sigma \sum_{k_\sigma=0}^\infty \int^{k_\sigma} d\boldsymbol{\tau}_\sigma \int^{k_\sigma} d\bar{\boldsymbol{\tau}}_\sigma\right) d^k_{\bar{\boldsymbol{\sigma}},\boldsymbol{\sigma}}(\boldsymbol{\tau},\bar{\boldsymbol{\tau}}) t^k_{\boldsymbol{\sigma},\bar{\boldsymbol{\sigma}}}(\boldsymbol{\tau},\bar{\boldsymbol{\tau}})$$

where the vectors $\boldsymbol{\sigma} = (\boldsymbol{\sigma}_\uparrow, \boldsymbol{\sigma}_\downarrow)$ and $\bar{\boldsymbol{\sigma}} = (\bar{\boldsymbol{\sigma}}_\uparrow, \bar{\boldsymbol{\sigma}}_\downarrow)$ have $(k_\uparrow, k_\downarrow)$ components, and for each k_σ component $\sigma_i = \bar{\sigma}_i = \sigma$. Thus

$$t^k_{\boldsymbol{\sigma},\bar{\boldsymbol{\sigma}}}(\boldsymbol{\tau},\bar{\boldsymbol{\tau}}) = {\rm Tr}_{\rm loc}\left(e^{-\beta(\hat{H}_{\rm loc}-\mu\hat{N}_d)}\,\mathcal{T}\prod\nolimits_\sigma\prod\nolimits^1_{i=k_\sigma} c_{d\sigma}(\tau_{\sigma_i}) c^\dagger_{d\sigma}(\bar{\tau}_{\bar{\sigma}_i})\right).$$

The latter can be calculated analytically. To do this, first we parametrize all configurations for a given spin via a timeline $[0,\beta)$ plus a number of creator/annihilator pairs which define segments

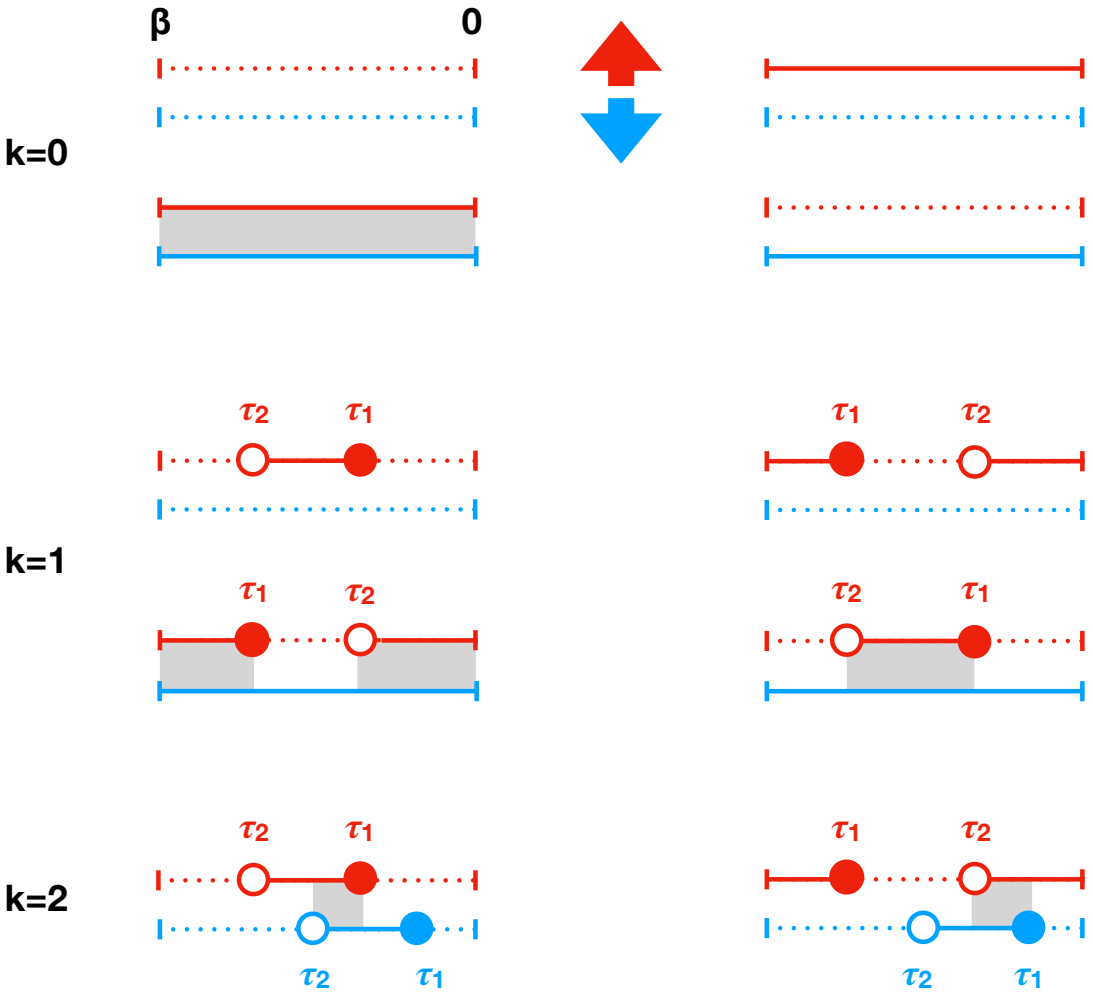

Fig. 3: *Representative configurations contributing to the local trace at zeroth, first and second order. The timelines for spin up are red and those for spin down are blue. The filled circles correspond to the insertion of a creator (time τ_1), and the empty circles to the insertion of an annihilator (time τ_2). Dotted lines represent the vacuum state for a given spin, full lines the occupied state. The grey boxes indicate the regions in which $l_{\uparrow,\downarrow} \neq 0$.*

on the timeline. At zeroth order two possible configurations exist per spin, an empty timeline, which corresponds to the vacuum state $|0\rangle$, and a full timeline, which corresponds to the state $c^\dagger_{d\sigma}|0\rangle$. A given configuration yields at order $k = k_\uparrow + k_\downarrow$

$$t^k_{\sigma,\bar{\sigma}}(\boldsymbol{\tau},\bar{\boldsymbol{\tau}}) = \left(\prod_\sigma s^{k_\sigma}_\sigma\right) e^{-\sum_{\sigma\sigma'}((\varepsilon_d-\mu)\delta_{\sigma\sigma'}+\frac{U}{2}(1-\delta_{\sigma,\sigma'}))l_{\sigma,\sigma'}}$$

where $l_{\sigma,\sigma'}$ is the length of the overlap of the τ segments for spins σ and σ', respectively, while $s_\sigma = \mathrm{sign}(\tau_{\sigma_1} - \bar{\tau}_{\sigma_1})$ is the fermionic sign. Possible configurations at order $k = 0, 1, 2$ are shown in Fig. 3. At order $k = 0$, summing up the contribution of the four configurations shown in Fig. 3 yields the local partition function $Z_{\mathrm{loc}} = 1 + 2e^{-\beta(\varepsilon_d-\mu)} + e^{-\beta(2(\varepsilon_d-\mu)+U)}$. Order $k = 1$

is already more complicated. The bath trace in this case is

$$d^1_{\bar\sigma\sigma}(\tau_1,\tau_2) = \mathcal{F}^0_{\bar\sigma\sigma}(\tau_1,\tau_2) = -\frac{t^2}{2}\delta_{\sigma,\bar\sigma}\ \mathrm{sign}(\tau_1-\tau_2).$$

The local trace is instead given by

$$t^1_{\sigma\bar\sigma}(\tau_2,\tau_1) = \mathrm{Tr}_{\rm loc}\Big(e^{-\beta(\hat H_{\rm loc}-\mu\hat N_d)}\mathcal{T}c_{d\sigma}(\tau_2)c^\dagger_{d\sigma}(\tau_1)\Big). \tag{7}$$

We can now calculate the contribution at half filling of the four $k=1$ configurations shown in Fig. 3. In the case $k_\uparrow = 1$ and $k_\downarrow = 0$ we have

$$t^1_{\uparrow\uparrow}(\tau_2,\tau_1) = \begin{cases} e^{-(\tau_2-\tau_1)(\varepsilon_d-\mu)} & = e^{+\tau_{21}U/2} \\ -e^{-\beta(2(\varepsilon_d-\mu)+U)+(\tau_1-\tau_2)(\varepsilon_d-\mu+U)} & = -e^{-\tau_{21}U/2} \\ -e^{-(\beta-(\tau_1-\tau_2))(\varepsilon_d-\mu)} & = -e^{(\beta+\tau_{21})U/2} \\ e^{-(\tau_2-\tau_1)(\varepsilon_d-\mu+U)-\beta(\varepsilon_d-\mu)} & = e^{(\beta-\tau_{21})U/2} \end{cases}$$

where $\tau_{21} = \tau_2 - \tau_1$ and $\mu = \varepsilon_d + U/2$. Similar results can be obtained for $k_\uparrow = 0$ and $k_\downarrow = 1$. Summing up all terms up to order one we find

$$\begin{aligned}\frac{Z}{Z_{\rm bath}} &\sim Z_{\rm loc} + \sum_\sigma \int_0^\beta d\tau_2 \int_0^\beta d\tau_1\, d^1_{\sigma\sigma}(\tau_1,\tau_2)t^1_{\sigma\sigma}(\tau_2,\tau_1) \\ &\sim Z_{\rm loc}\left(1 - \frac{1-e^{\frac{\beta U}{2}}}{1+e^{\frac{\beta U}{2}}}\frac{2t^2}{U}\beta\right).\end{aligned}$$

The exact formula of the partition function can be obtained from the eigenvalues and eigenvectors in the Appendix A.2; its Taylor expansion in powers of t/U yields, at second order, the expression above. Eq. (7) shows in addition that, for $k=1$, the local trace is proportional to the local Green function, $G^\sigma_{d,d}(\tau)$. Indeed, $G^\sigma_{d,d}(\tau)$ can be calculated using the configurations just described—provided that we start from $k=1$ and we divide by the hybridization function. More specifically, for $k=1$ and $\tau > 0$ we have

$$G^\sigma_{d,d}(\tau) \sim -\frac{1}{\beta}\int_0^\beta\int_0^\beta \underbrace{d\tau_2 d\tau_1\ d^1_{\sigma\sigma}(\tau_1,\tau_2)t^1_{\sigma\sigma}(\tau_2,\tau_1)}_{w^1}\ \delta\big(\tau-(\tau_2-\tau_1)\big)\ \frac{1}{\mathcal{F}^0_{\sigma\sigma}(\tau_1-\tau_2)}.$$

Taking all k values into account, the partition function can be expressed as the sum over all configurations $\{c\}$, i.e., in short

$$Z = \sum_c w_c = \sum_c |w_c|\ \mathrm{sign}\ w_c.$$

In a compact form, we can write $w_c = d\boldsymbol{\tau}_c\ d_c\ t_c$ where $d\boldsymbol{\tau}_c = \prod_\sigma \prod_i^{k_\sigma} d\tau_{\sigma_i} d\bar\tau_{\bar\sigma_i}$, and d_c and t_c are the bath and local traces for the configuration c. This expression of the partition function

shows that we can interpret $|w_c|$ as the sampling weight of configuration c. A generic observable $\hat{O}$ can then be obtained as the Monte Carlo average on a finite number of configurations N_c

$$\langle \hat{O} \rangle = \frac{\sum_c \langle \hat{O} \rangle_c |w_c| \,\mathrm{sign}\, w_c}{\sum_c |w_c| \,\mathrm{sign}\, w_c} = \frac{\sum_c \mathrm{sign}\, w_c \langle \hat{O} \rangle_c \, |w_c| / \sum_c |w_c|}{\sum_c \mathrm{sign}\, w_c \, |w_c| / \sum_c |w_c|} \approx \frac{\frac{1}{N_c} \sum_c^{N_c} \langle \hat{O} \rangle_c \mathrm{sign}\, w_c}{\frac{1}{N_c} \sum_c \mathrm{sign}\, w_c}.$$

The term $\frac{1}{N_c} \sum_c \mathrm{sign}\, w_c$ in the denominator is the average fermionic sign. When this is small, much longer runs are required to obtain data of the same quality; eventually the computational time can become so long that the calculation is in practice impossible—in these cases we have a sign problem. In practice, the QMC simulation starts from a random configuration c. Next we propose an update $c \to c'$. Within the Metropolis algorithm, the acceptance ratio is

$$R_{c \to c'} = \min\left(1, \frac{p_{c' \to c}}{p_{c \to c'}} \frac{|w_{c'}|}{|w_c|}\right)$$

where $p_{c \to c'}$ is the proposal probability for the update $c \to c'$. In the approach described here, known as *segment solver*, the basic updates are addition and removal of segments, antisegments (segments winding over the borders of the timeline, see Fig. 3), or complete lines. As example, let us consider the insertion of a segment for spin σ. A segment is made by a creator and an annihilator. The creator is inserted at time $\tau_{\rm in}$; the move is rejected if $\tau_{\rm in}$ is in a region where a segment exists. If created, the segment can have at most length $l_{\rm max}$, given by the distance between $\tau_{\rm in}$ and the time at which the next creator is, hence

$$p_{c \to c'} = \frac{d\bar{\tau}}{\beta} \frac{d\tau}{l_{\rm max}} \,.$$

The proposal probability of the reverse move (removing a segment) is instead given by the inverse of the number of existing segments

$$p_{c' \to c} = \frac{1}{k_\sigma + 1}$$

The acceptance ratio for the insertion of a segment becomes then

$$R_{c \to c'} = \min\left(1, \frac{\beta l_{max}}{k_\sigma + 1} \left| \frac{d_{c'}}{d_c} \frac{t_{c'}}{t_c} \right| \right).$$

For the impurity Green function, here the most important observable, the direct average yields

$$\langle \hat{O} \rangle_c = \langle G^\sigma_{d,d} \rangle_c = \sum_{\sigma'} \sum_{i=1}^{k_\sigma} \sum_{j=1}^{k_\sigma} \Delta(\tau, \tau_{\sigma' j} - \bar{\tau}_{\sigma' j}) \left(M^{k'_\sigma}\right)_{\sigma' j, \sigma' i} \delta_{\sigma, \sigma_{\sigma' j}} \delta_{\sigma, \bar{\sigma}_{\sigma' i}}$$

where $M^k = \left(\mathcal{F}^k\right)^{-1}$ is the inverse of the hybridization matrix and

$$\Delta(\tau, \tau') = -\frac{1}{\beta} \begin{cases} \delta(\tau - \tau') & \tau' > 0 \\ -\delta(\tau - (\tau' + \beta)) & \tau' < 0 \end{cases} .$$

2.4 DMFT for the one-band Hubbard model

The Hubbard Hamiltonian (3) is in principle the simplest model for the description of the Mott metal-insulator transition. In the tight-binding approximation it becomes

$$\hat{H} = \varepsilon_d \sum_{\sigma i} \hat{n}_{i\sigma} - t \sum_{\sigma \langle ii' \rangle} c^\dagger_{i\sigma} c_{i'\sigma} + U \sum_i \hat{n}_{i\uparrow} \hat{n}_{i\downarrow}, \tag{8}$$

where $\langle ii' \rangle$ is a sum over first neighbors. As discussed in the introduction, for $U = 0$, at half-filling, this Hamiltonian describes a metallic band. For $t = 0$ it describes an insulating collection of disconnected atoms. Somewhere in between, at a critical value of t/U, a metal to insulator transition must occur. In this section we will discuss the DMFT solution of (8) and the picture of the metal-insulator transition emerging from it. The first step consists in mapping the original many-body Hamiltonian into an effective quantum-impurity model, such as the Anderson Hamiltonian

$$\hat{H}^A = \underbrace{\sum_{\boldsymbol{k}\sigma} \varepsilon^s_{\boldsymbol{k}} \hat{n}_{\boldsymbol{k}\sigma}}_{\hat{H}_{\rm bath}} + \underbrace{\sum_{\boldsymbol{k}\sigma} \left(V^s_{\boldsymbol{k}} c^\dagger_{\boldsymbol{k}\sigma} c_{d\sigma} + \text{h.c.} \right)}_{\hat{H}_{\rm hyb}} + \underbrace{\varepsilon_d \sum_\sigma \hat{n}_{d\sigma} + U \hat{n}_{d\uparrow} \hat{n}_{d\downarrow}}_{\hat{H}_{\rm imp}}.$$

In this model the on-site Coulomb repulsion U appears only in the impurity Hamiltonian, $\hat{H}_{\rm imp}$, while the terms $\hat{H}_{\rm bath}$ and $\hat{H}_{\rm hyb}$, describe, respectively, the bath and the bath-impurity hybridization. In the next step, the quantum-impurity model is solved. Differently from the case of the Anderson molecule, this cannot be done analytically. It requires non-perturbative numerical methods, such as exact diagonalization, the numerical renormalization group, or QMC. Here we describe the DMFT self-consistency loop for a QMC quantum-impurity solver. Solving the quantum-impurity model yields the impurity Green function $G^\sigma_{d,d}(i\nu_n)$. From the impurity Dyson equation we can calculate the impurity self-energy

$$\Sigma^\sigma_A(i\nu_n) = \left(G^{0\sigma}_{d,d}(i\nu_n) \right)^{-1} - \left(G^\sigma_{d,d}(i\nu_n) \right)^{-1}.$$

Next, we adopt the local approximation, i.e., we assume that the self-energy of the Hubbard model equals the impurity self-energy. Then, the local Green function is given by

$$G^\sigma_{i_c,i_c}(i\nu_n) = \frac{1}{N_{\boldsymbol{k}}} \sum_{\boldsymbol{k}} \frac{1}{i\nu_n + \mu - \varepsilon_{\boldsymbol{k}} - \Sigma^\sigma_A(i\nu_n)},$$

where $N_{\boldsymbol{k}}$ is the number of $\boldsymbol{k}$ points. The local Dyson equation is used once more, this time to calculate the bath Green function $\mathcal{G}^\sigma(i\nu_n)$, which in turn defines a new quantum-impurity model. This procedure is repeated until self-consistency is reached, i.e., the number of electrons is correct and the self-energy does not change anymore (within a given numerical accuracy). In this situation we have

$$G^\sigma_{i_c,i_c}(i\nu_n) \sim G^\sigma_{d,d}(i\nu_n).$$

It is important to underline that self-consistency is key to the success of DMFT in describing the metal-to-insulator transition. This can, perhaps, be best understood looking at the effects of

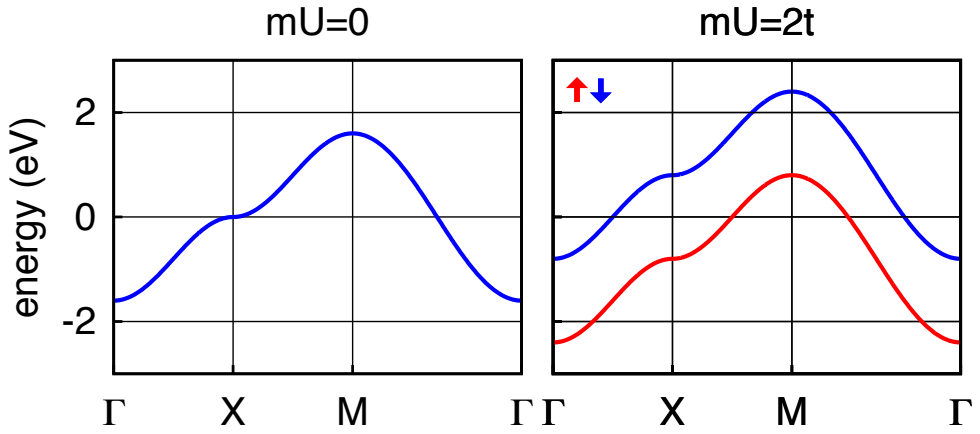

Fig. 4: *The metal-insulator transition in ferromagnetic Hartree-Fock. The calculation is for a square lattice tight-binding model with dispersion* $\varepsilon_{\boldsymbol{k}} = -2t(\cos k_x + \cos k_y)$.

self-consistency in a simpler approach, the static mean-field Hartree-Fock method.[6] The latter consists in replacing the Coulomb interaction with the one-electron operator

$$U\hat{n}_{i\uparrow}\hat{n}_{i\downarrow} \to U(\hat{n}_{i\uparrow}\bar{n}_{i\downarrow} + \bar{n}_{i\uparrow}\hat{n}_{i\downarrow} - \bar{n}_{i\uparrow}\bar{n}_{i\downarrow}),$$

where $\bar{n}_{i\sigma}$ is the expectation value of $\hat{n}_{i\sigma}$. Choosing the same primitive cell as in dynamical mean-field theory ($\bar{n}_{i\sigma} = \bar{n}_\sigma$), the Hartree-Fock self-energy matrix is given by

$$\Sigma^\sigma_{i,i'}(i\nu_n) = U\Big(\frac{n}{2} - \sigma m\Big)\delta_{i,i'},$$

where $\sigma = +1$ for spin up and $\sigma = -1$ for spin down and $m = (\bar{n}_\uparrow - \bar{n}_\downarrow)/2$. The approximation is then identical to replacing the Hubbard Hamiltonian with

$$\hat{H}_{\rm HF} = \sum_{\boldsymbol{k}\sigma}\left[\varepsilon_{\boldsymbol{k}} + U\left(\frac{1}{2} - \sigma m\right)\right]\hat{n}_{\boldsymbol{k}\sigma}. \tag{9}$$

This shows that $h_{\rm eff} = 2Um$ plays the role of an effective magnetic field (Weiss field). The self-consistency criterion is

$$\bar{n}_\sigma = \bar{n}_{i\sigma} = \langle\hat{n}_{i\sigma}\rangle_{\rm HF},$$

where the expectation value $\langle\hat{n}_{i\sigma}\rangle_{\rm HF}$ is calculated using the Hamiltonian $\hat{H}_{\rm HF}$, which in turn depends on $\bar{n}_\sigma$ via m. This gives the self-consistency equation

$$m = \frac{1}{2}\frac{1}{N_{\boldsymbol{k}}}\sum_{\boldsymbol{k}\sigma}\frac{\sigma e^{-\beta(\varepsilon_{\boldsymbol{k}}+U(\frac{1}{2}-\sigma m)-\mu)}}{1+e^{-\beta(\varepsilon_{\boldsymbol{k}}+U(\frac{1}{2}-\sigma m)-\mu)}}.$$

If we set $m = 0$ the equation is satisfied; for such a trivial solution the static mean-field correction in Eq. (9) merely redefines the chemical potential and has therefore no effect. For sufficiently large U, however, a non-trivial solution ($m \neq 0$) can be found. If $m \neq 0$ the spin up and spin down bands split, and eventually a gap can open. This is shown in Fig. 4. The static mean-field correction in Eq. (9) equals the contribution of the Hartree diagram to the self-energy, $\Sigma^\sigma_{\rm H}(i\nu_n) = U\bar{n}_{-\sigma}$. In many-body perturbation theory, however, $\bar{n}_\sigma = 1/2$, i.e., $m = 0$.

[6] Keeping in mind that many self-consistent solutions obtained with the Hartree-Fock method are spurious.

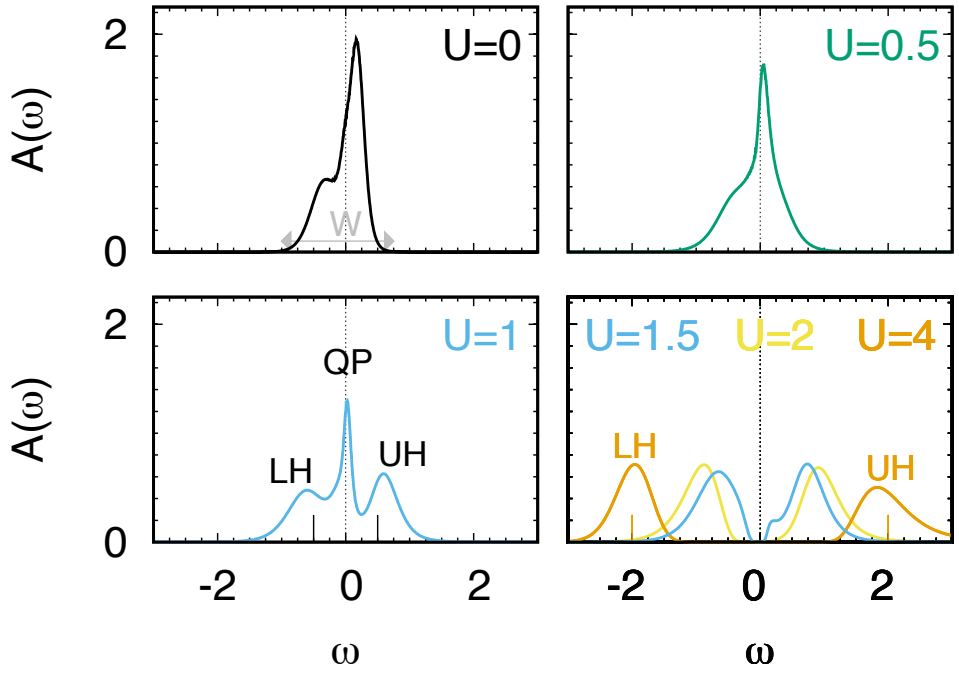

Fig. 5: *$VOMoO_4$: LDA+DMFT spectral function at finite temperature for $0 \leq U \leq 4$. Energies are in eV and spectral functions in states/spin/eV. The calculations have been done using a continuous-time hybridization-expansion QMC solver [10]. A detailed LDA+DMFT study of the electronic and magnetic properties $VOMoO_4$ can be found in Ref. [11].*

In the self-consistent static mean-field approximation, instead, m can differ from zero, and a phenomenon not described by the mere Hartree diagram can be captured, ferromagnetism in a correlated metal. If mU is larger than the bandwidth, the system can even become an insulator. In DMFT the role of the Weiss field is played by the bath Green function $\mathcal{G}^{\sigma}_{i,i}(i\nu_n)$. The emerging picture of the Mott transition is described in Fig. 5 for a representative single-band material. In the $U = 0$ limit, the spectral function $A_0(\omega)$ is metallic at half filling (top left panel). For finite U, if we set $\Sigma^{\sigma}_A(\omega) = 0$ as initial guess, the DMFT self-consistency loop starts with $A(\omega) = A_0(\omega)$. For small U/t, the *converged* spectral function $A(\omega)$ is still similar to $A_0(\omega)$. This can be seen comparing the $U = 0.5$ and $U = 0$ panels in Fig. 5. Further increasing U/t, sizable spectral weight is transferred from the zero-energy quasi-particle peak to the lower (LH) and upper (UH) Hubbard bands, centered at $\omega \sim \pm U/2$. This can be observed in the $U = 1$ panel of Fig. 5. The system is still metallic, but with strongly renormalized masses and short lifetimes, reflected in the narrow quasi-particle (QP) peak. Finally, for U larger than a critical value ($U \geq 1.5$ in the figure) a gap opens and the system becomes a Mott insulator. When this happens the self-energy diverges at low frequency, where

$$\Sigma^{\sigma}_A(\omega+i0^+) \sim \frac{U}{2} + \frac{A}{\omega + i0^+}.$$

In the large U/t limit the gap increases linearly with the Coulomb repulsion, i.e., $E_g(1) \sim U - W$, where W is the bandwidth.

2.5 DMFT for multi-orbital models

The multi-orbital Hubbard-like Hamiltonian has the form

$$\hat{H} = \hat{H}_0 + \hat{H}_U$$
$$\hat{H}_0 = -\sum_{ii'}\sum_{\sigma}\sum_{mm'} t^{i,i'}_{m\sigma,m'\sigma'}\, c^{\dagger}_{im\sigma} c_{i'm'\sigma'}$$
$$\hat{H}_U = \frac{1}{2}\sum_{i}\sum_{\sigma\sigma'}\sum_{mm'}\sum_{pp'} U_{mpm'p'}\, c^{\dagger}_{im\sigma} c^{\dagger}_{ip\sigma'} c_{ip'\sigma'} c_{im'\sigma},$$

where m, m' and p, p' are different orbitals and the Coulomb tensor is local. The DMFT approach can be extended to solve models of this form, mapping them to multi-orbital quantum-impurity models. The main changes with respect to the formalism introduced in the previous section are then the following

$$\varepsilon_{\boldsymbol{k}} \to (H_{\boldsymbol{k}})_{m\sigma,m'\sigma'} \qquad (i\nu_n + \mu) \to (i\nu_n + \mu)\,\hat{1}_{m\sigma,m'\sigma'}$$
$$t^{i,i'} \to t^{i,i'}_{m\sigma,m'\sigma'} \qquad \varepsilon_d \to \varepsilon^{i,i'}_{m\sigma,m'\sigma'} = -t^{i,i}_{m\sigma,m'\sigma'}$$

where $\hat{1}$ is the identity matrix. As a consequence, the local Green function, the bath Green function, the hybridization function and the self-energy also become matrices

$$\mathcal{G}^{\sigma}(i\nu_n) \to \mathcal{G}^{\sigma,\sigma'}_{m,m'}(i\nu_n) \qquad G^{\sigma}(i\nu_n) \to G^{\sigma,\sigma'}_{m,m'}(i\nu_n) \qquad \Sigma^{\sigma}(i\nu_n) \to \Sigma^{\sigma,\sigma'}_{m,m'}(i\nu_n).$$

The corresponding generalization of the self-consistency loop is shown schematically in Fig. 6. Although the extension of DMFT to Hubbard models with many orbitals might appear straightforward, in practice it is not. The bottleneck is the solution of the generalized multi-orbital quantum-impurity problem. The most flexible solvers available so far are all based on QMC. Despite being flexible, QMC-based approaches have limitations. These can be classified in two types. First, with increasing the number of degrees of freedom, calculations become very quickly computationally too expensive—how quickly depends on the specific QMC algorithm used and the actual implementation. Thus, going beyond a rather small number of orbitals and reaching the zero-temperature limit is unfeasible in practice. The second type of limitation is more severe. Increasing the number of degrees of freedom leads, eventually, to the infamous sign problem; when this happens, QMC calculations cannot be performed at all. In order to deal with limitations of the first type, it is crucial to restrict QMC calculations to the essential degrees of freedom; furthermore, we should exploit symmetries, develop fast algorithms and use the power of massively parallel supercomputers to reduce the actual computational time. For the second type of problems not a lot can be done; nevertheless, it has been shown that a severe sign problem might appear earlier with some basis choices than with others [10]. Although eventually we cannot escape it, this suggests that the model set up can be used as a tool to expand the moderate sign-problem zone. For what concerns symmetries, in the paramagnetic case and in absence of spin-orbit interaction or external fields, an obvious symmetry to exploit

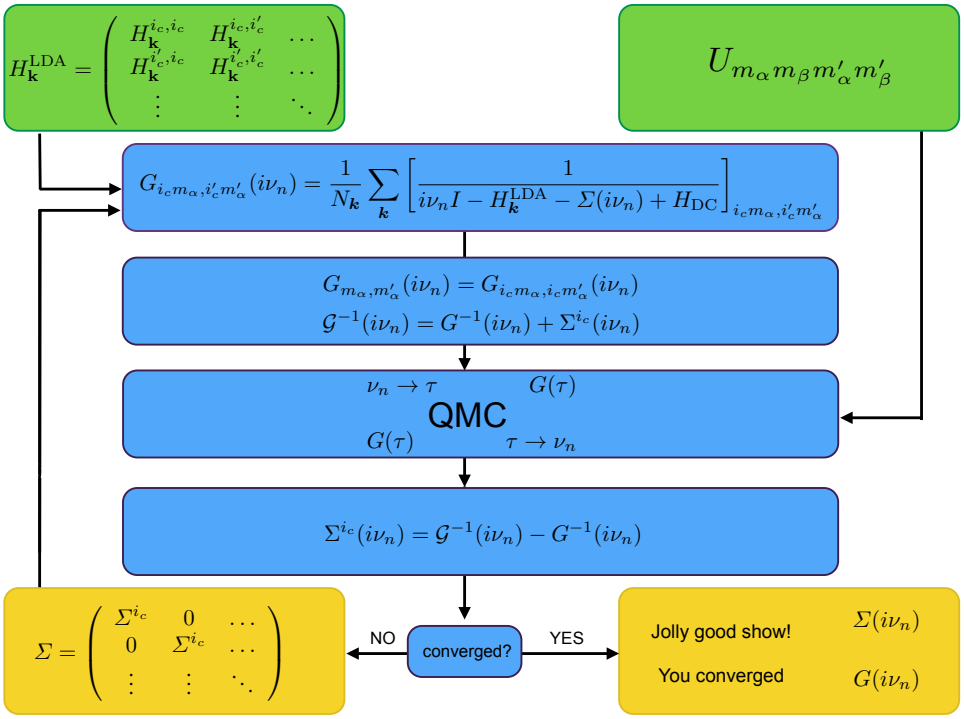

Fig. 6: *LDA+DMFT self-consistency loop. The one-electron Hamiltonian is built in the basis of Bloch states obtained from localized Wannier functions, for example in the local-density approximation (LDA); this gives* $H_{\boldsymbol{k}}^{\mathrm{LDA}}$*. The set* $\{i_c\}$ *labels the equivalent correlated sites inside the unit cell. The local Green-function matrix is at first calculated using an initial guess for the self-energy matrix. The bath Green-function matrix is then obtained via the Dyson equation and used to construct an effective quantum-impurity model. The latter is solved via a quantum-impurity solver, here quantum Monte Carlo (QMC). This yields the impurity Green-function matrix. Through the Dyson equation the self-energy is then obtained, and the procedure is repeated until self-consistency is reached.*

is the rotational invariance of spins, from which follows

$$X^{\sigma,\sigma'}_{m,m'}(i\nu_n) = \delta_{\sigma,\sigma'}\, X_{m,m'}(i\nu_n),$$

where $X = \mathcal{G}, G, \Sigma$. In addition, if we use a basis of real functions, the local Green-function matrices are real and symmetric in imaginary time τ, hence

$$X^{\sigma,\sigma'}_{m,m'}(i\nu_n) = \delta_{\sigma,\sigma'}\, X_{m,m'}(i\nu_n) = \delta_{\sigma,\sigma'}\, X_{m',m}(i\nu_n).$$

Finally, often the unit cell contains several equivalent correlated sites, indicated as $\{i_c\}$ in Fig. 6. In order to avoid expensive cluster calculations, we can use space-group symmetries to construct the matrices $\mathcal{G}, G, \Sigma$ at a given site i'_c from the corresponding matrices at an equivalent site, e.g., $i_c = 1$. Space-group symmetries also tell us if some matrix elements are zero. For example, for a model with only t_{2g} (or only e_g) states, in cubic symmetry, in the paramagnetic case and in absence of spin-orbit interaction or external fields, we have

$$X^{\sigma,\sigma'}_{m,m'}(i\nu_n) = \delta_{\sigma,\sigma'}\, X_{m,m}(i\nu_n)\, \delta_{m,m'}.$$

2.6 LDA+DMFT: Model building

How do we build realistic Hubbard-like models for correlated materials? The state-of-the art approach relies on constructing, for a given system, *materials-specific* Kohn-Sham Wannier functions $\phi^{\rm KS}_{im\sigma}(\boldsymbol{r})$. These can be obtained via electronic structure calculations based on density-functional theory [5–7], e.g., in the LDA approximation.[7] After we have built the complete one-electron basis, the first steps in model-building are those already described in the introduction. We recall here the essential points and then discuss the next stage. The many-body Hamiltonian can be expressed as $\hat{H} = \hat{H}_0 + \hat{H}_U - \hat{H}_{\rm DC}$, with

$$\hat{H}_0 = \hat{H}^{\rm LDA} = -\sum_{\sigma}\sum_{ii'}\sum_{mm'} t^{i,i'}_{m,m'} c^\dagger_{im\sigma} c_{i'm'\sigma},$$

$$\hat{H}_U = \frac{1}{2}\sum_{ii'jj'}\sum_{\sigma\sigma'}\sum_{mm'pp'} U^{iji'j'}_{mp\,m'p'} c^\dagger_{im\sigma} c^\dagger_{jp\sigma'} c_{j'p'\sigma'} c_{i'm'\sigma}.$$

The double-counting correction $\hat{H}_{\rm DC}$ arises from the fact that the hopping integrals are calculated replacing the electron-nuclei interaction $v_{\rm en}(\boldsymbol{r})$ with the self-consistent DFT reference potential

$$v_{\rm R}(\boldsymbol{r}) = v_{\rm en}(\boldsymbol{r}) + \underbrace{\int d\boldsymbol{r}'\, \frac{1}{|\boldsymbol{r}-\boldsymbol{r}'|}}_{v_{\rm H}(\boldsymbol{r})} + v_{\rm xc}(\boldsymbol{r}),$$

which includes the long-range Hartree term $v_{\rm H}(\boldsymbol{r})$ and the exchange-correlation contribution $v_{\rm xc}(\boldsymbol{r})$. To avoid to count these terms twice, we thus subtract from $\hat{H}_U$ the effects already included in $\hat{H}_0$

$$\hat{H}_U \to \Delta\hat{H}_U = \hat{H}_U - \hat{H}_{\rm DC}.$$

Unfortunately we do not know which important correlation effects are indeed included in $\hat{H}_0$ via $v_{\rm R}(\boldsymbol{r})$, and therefore the exact expression of $\Delta\hat{H}_U$ is also unknown. The remarkable successes of the LDA suggest, however, that in many materials the LDA is overall a good approximation, and therefore, in those systems at least, the term $\Delta\hat{H}_U$ can be completely neglected. What about strongly-correlated materials? Even in correlated systems, most likely the LDA works rather well for the delocalized electrons or in describing the average or the long-range Coulomb effects. Thus one can think of separating the electrons into *uncorrelated* and *correlated*; only for the latter we do take the correction $\Delta\hat{H}_U$ into account explicitly, assuming furthermore that $\Delta\hat{H}_U$ is local or almost local [5], since we know that it is the local term which is responsible for most non-trivial many-body effects. Typically, correlated electrons are those that partially retain their atomic character, e.g., those that originate from localized d and f shells; for convenience, here we assume that in a given system they stem from a single atomic shell l (e.g., d for

[7] Using GGA or similar functionals in place of LDA yields minor differences in the many-body Hamiltonian; instead, using LDA+U or similar approximations yields Hartree-Fock-like effects that would have to be subtracted via the double-counting correction.

transition-metal oxides or f for heavy-fermion systems) and label their states with the atomic quantum numbers l and $m = -l, \ldots, l$ of that shell. Thus

$$U^{iji'j'}_{mp\,m'p'} \sim \begin{cases} U^l_{mp\,m'p'} & iji'j' = iiii \quad \wedge \quad mp, m'p' \in l \\ 0 & iji'j' \neq iiii \quad \vee \quad mp, m'p' \notin l. \end{cases}$$

Within this approximation $\Delta\hat{H}_U$ is replaced by $\Delta\hat{H}^l_U = \hat{H}^l_U - \hat{H}^l_{\rm DC}$, where $\hat{H}^l_{\rm DC}$ is, e.g., given by the static mean-field contribution of $\hat{H}^l_U$. There is a drawback in this procedure, however. By splitting electrons into correlated and uncorrelated we implicitly assume that the main effect of the latter is the renormalization or *screening* of parameters for the former, in particular of the Coulomb interaction. The computation of screening effects remains, unfortunately, a challenge. The calculation of exact screening would require the solution of the original many-body problem, taking all degrees of freedom into account, an impossible task. Commonly-used approximate schemes are the constrained LDA approximation (cLDA) and the constrained random-phase approximation (RPA) [5–7]. Both methods give reasonable estimates of screened Coulomb parameters for DMFT calculations. Typically cRPA calculations include more screening channels and are performed for less localized bases than cLDA calculations; thus cRPA parameters turn out to be often smaller than cLDA ones. To some extent, the difference can be taken as an estimate of the error bar.

After we have selected the electrons for which we think it is necessary to include explicitly the Hubbard correction, we have to build the final Hamiltonian for DMFT calculations. To this end, it is often convenient to integrate out or *downfold*, in part or completely, the weakly correlated states. There are different degrees of downfolding. The two opposite extreme limits are (i) *no downfolding*, i.e., keep explicitly in the Hamiltonian all weakly-correlated states (ii) *massive downfolding*, i.e., downfold all weakly correlated states. If we perform massive downfolding, e.g., downfold to the d (or e_g or t_{2g}) bands at the Fermi level, the Hamiltonian relevant for DMFT takes a simpler form. The LDA part is limited to the selected orbitals or bands, which, in the ideal case, are decoupled from the rest

$$\hat{H}^{\rm LDA} = -\sum_{\sigma} \sum_{ii'} \sum_{m_\alpha m'_\alpha} t^{i,i'}_{m_\alpha, m'_\alpha}\, c^\dagger_{im_\alpha\sigma}\, c_{i'm'_\alpha\sigma}.$$

The local *screened* Coulomb interaction for this set of orbitals is the on-site tensor

$$\hat{H}^l_U = \frac{1}{2} \sum_{i} \sum_{\sigma\sigma'} \sum_{m_\alpha m'_\alpha} \sum_{m_\beta m'_\beta} U_{m_\alpha m_\beta m'_\alpha m'_\beta}\, c^\dagger_{im_\alpha\sigma} c^\dagger_{im_\beta\sigma'} c_{im'_\beta\sigma'} c_{im'_\alpha\sigma}.$$

It is important to point out that the level of downfolding does not modify the hardness of the quantum-impurity problem. If, for example, in studying a transition-metal oxide, we plan to treat only $3d$ bands as correlated, it does not matter if we perform calculations with a Hamiltonian containing also, e.g., O p states, or we rather downfold all states but the $3d$ and work with a set of Wannier basis spanning the $3d$-like bands only. The number of correlated orbitals in the quantum-impurity problem is the same.[8]

[8] The choice might influence how severe the QMC sign problem is, however.

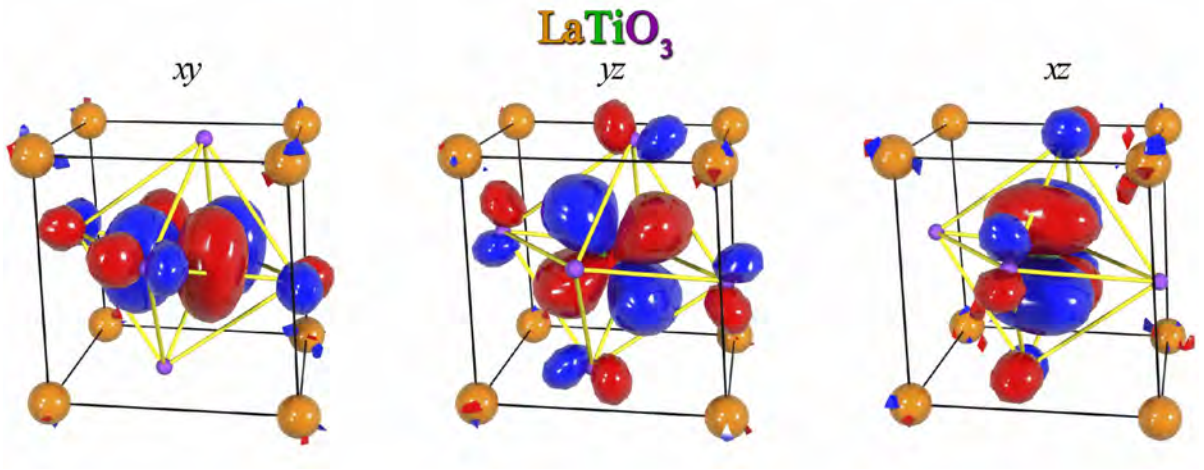

Fig. 7: *NMTO Wannier-like orbitals for t_{2g} states in $LaTiO_3$ obtained via massive downfolding to the t_{2g} bands. The t_{2g}-like orbitals have O p tails at the neighboring O sites reflecting the distortions of the lattice. The figure has been taken from Ref. [12].*

One advantage of massive downfolding is that the double-counting correction typically becomes a shift of the chemical potential, and it is therefore not necessary to calculate it explicitly. A second important advantage is that the interpretation of the final results is simpler. Instead, a disadvantage is that the basis functions are less localized, and therefore the approximation of the Coulomb interaction to a local operator might be less justified, and in some cases it might be necessary to include non-local Coulomb terms. The effect of downfolding on the localization of Wannier functions is illustrated for example in Fig. 7. Finally, another disadvantage of massive downfolding is that the energy window in which the model is valid is more narrow.

All advantages and disadvantages considered, what is then the best way of performing DMFT calculations? There is no universal answer to this question; it depends on the problem we are trying to solve and the system we are studying. Independently of the degree of downfolding we choose, it is important to point out that a clear advantage of Wannier functions in general is that they carry information about the lattice, bonding, chemistry, and distortions. This can be seen once more in Fig. 7, where orbitals are tilted and deformed by the actual structure and chemistry of the compound. Indeed, one might naively think of using an "universal" basis, for example atomic functions, the same for all systems, and thus calculating the hopping integrals using simply the electron-nuclear interaction $v_{en}(\boldsymbol{r})$. Besides the complications arising from the lack of orthogonality, such a basis has no built-in materials-specific information, except lattice positions. It is therefore a worse starting point for describing the electronic structure, even in the absence of correlations: larger basis sets are required to reach the same accuracy. From the point of view of LDA+DMFT, an advantage of an universal basis would be that it is free from double-counting corrections; on the other hand, however, exactly because we do not use the LDA potential and LDA orbitals to calculate the hopping integrals, we also cannot count on the successes of LDA in the description of average and long-range Coulomb effects. The hopping integrals would not even include the long-range Hartree term. For these

reasons *ab-initio* Wannier functions remain so far the basis of choice. They can be built via the Nth-Order Muffin-Tin Orbital (NMTO) method [12], the maximal-localization scheme [13], or projectors. Fig. 7 shows examples of NMTO-based Wannier functions. No matter what construction procedure is used, a common characteristic of *ab-initio* Wannier functions is that they are site-centered and localized.[9] A question naturally arises: How crucial is it to use localized functions as one-electron basis? This is an important point, since we have seen that strong-correlation effects arise in systems in which the on-site Coulomb interaction is much larger than longer-range terms. Let us consider therefore two opposite extreme limits. The first is the case in which the basis functions are independent of the lattice position (i.e., they are totally delocalized). For such a basis choice the Coulomb interaction parameters would be the same for every pair of lattice sites, no matter how distant. Thus a Hubbard-like model would be hard to justify. In the second extreme case, we adopt a hypothetical basis so localized that $\psi_{im\sigma}(\boldsymbol{r})\overline{\psi_{i'm'\sigma'}}(\boldsymbol{r}) \sim \delta_{i,i'}\,\delta(\boldsymbol{r}-\boldsymbol{T}_i)$. Even for such a basis choice, the unscreened Coulomb interaction is *not* local, but given by

$$U^{iji'j'}_{mp\,m'p'} \propto \frac{\delta_{i,i'}\delta_{j,j'}}{|\boldsymbol{T}_i-\boldsymbol{T}_j|},$$

hence it decays slowly with distance, although the (divergent) on-site term dominates. More generally, we can conclude that by increasing the localization of the basis we enhance the importance of the on-site Coulomb repulsion with respect to long-range terms; this better justifies Hubbard-like models—although we have to remember that most of the long-range part of the Coulomb interaction is in any case subtracted via the double-counting correction $\hat{H}_{\rm DC}$. The extreme case of the $\delta(\boldsymbol{r}-\boldsymbol{T}_i)$ functions also illustrates, however, how far we can go. A major problem with the extremely localized basis discussed above is that it would make it impossible to properly describe bonding, since the hopping integrals would be zero. Although such a basis is, of course, never used to build many-body models, there is a tempting approximation that has similar flaws. If one uses DFT-based electronic-structure techniques that tile the space in interstitial and non-overlapping atomic spheres (e.g., the LAPW method), it is tempting to use as basis for correlated electrons the atomic functions *defined inside the atomic spheres*. These functions are, by construction, much more localized than Wannier orbitals (even when no downfolding is performed in the Wannier construction). However, they *do not form a complete basis set* in the space of square-integrable functions. This is obvious because such a basis does not even span the LDA bands; to reproduce the bands we need, in addition, functions defined in the interstitial region. This is illustrated in Fig. 8 for a simple example of two quantum well potentials.[10] We therefore cannot use it to write the many-body Hamiltonian in the usual form $\hat{H}_0 + \hat{H}_U$. In conclusion, a basis which, as *ab-initio* Wannier functions, is complete and indeed spans the bands, is better justified, although we somewhat lose in localization.

[9] Differences in localizations between the various construction procedures are actually small for the purpose of many-body calculations, provided that the same bands are spanned in the same way.

[10] Another, but less severe, problem of atomic sphere truncations is that the results will depend on the sphere size, in particular when atomic spheres are small.

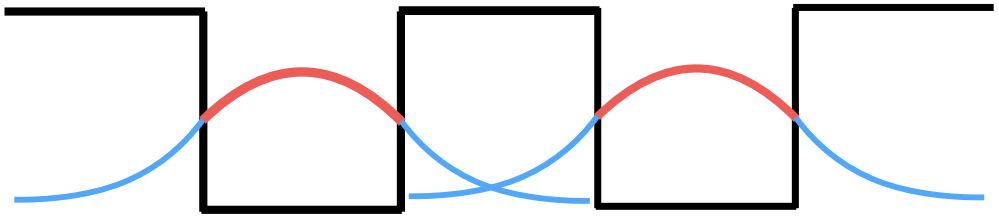

Fig. 8: *The problem of two quantum wells. The figure shows (schematically) for each well the wavefunction of a bound state. If we consider only the part of the wavefunction inside its own well (red in the figure), the differential overlap (and hence the hopping integral) between functions centered on different wells would be zero.*

3 Linear response functions

Linear response functions are key to understand many experimental results. In this section we explain how to calculate them within the LDA+DMFT approach. First we introduce the generalized susceptibility, which yields the linear response to a given external perturbation. Next we present the method used to calculate it and discuss the approximations adopted. Last we analyze in detail the case of the magnetic susceptibility for the one-band Hubbard model.

3.1 The generalized susceptibility

Let us start by introducing the site susceptibility in imaginary time. This is given by

$$\chi_{\hat{P}^i_\nu\,\hat{O}^{i'}_{\nu'}}(\boldsymbol{\tau}) = \left\langle \mathcal{T}\Delta\hat{P}^i_\nu(\tau_1,\tau_2)\Delta\hat{O}^{i'}_{\nu'}(\tau_3,\tau_4)\right\rangle_0, \tag{10}$$

where $\boldsymbol{\tau} = (\tau_1,\tau_2,\tau_3,\tau_4)$. The site operators are defined via the equations

$$\hat{P}^i_\nu(\tau_1,\tau_2) = \sum_{\boldsymbol{\alpha}} p^\nu_{\boldsymbol{\alpha}}\; c^\dagger_{i\alpha'}(\tau_2)c_{i\alpha}(\tau_1), \qquad \Delta\hat{P}^i_\nu(\tau_1,\tau_2) = \hat{P}^i_\nu(\tau_1,\tau_2) - \langle\hat{P}^i_\nu(\tau_1,\tau_2)\rangle$$
$$\hat{O}^{i'}_{\nu'}(\tau_3,\tau_4) = \sum_{\boldsymbol{\gamma}} o^{\nu'}_{\boldsymbol{\gamma}}\; c^\dagger_{i'\gamma'}(\tau_4)c_{i'\gamma}(\tau_3), \qquad \Delta\hat{O}^{i'}_{\nu'}(\tau_3,\tau_4) = \hat{O}^{i'}_{\nu'}(\tau_3,\tau_4) - \langle\hat{O}^{i'}_{\nu'}(\tau_3,\tau_4)\rangle.$$

The labels $\boldsymbol{\alpha} = (\alpha,\alpha')$, $\boldsymbol{\gamma} = (\gamma,\gamma')$ are collective flavors. For the multi-band Hubbard model they may include spin (σ) and orbital (m) quantum number, plus a fractional lattice vector identifying a correlated basis atom in the unit cell (i_c). The weight factors $o^\nu_{\boldsymbol{\alpha}}$ and $p^{\nu'}_{\boldsymbol{\gamma}}$, in general complex numbers, identify the type of response. We can then rewrite Eq. (10) as

$$\chi_{\hat{P}^i_\nu\,\hat{O}^{i'}_{\nu'}}(\boldsymbol{\tau}) = \sum_{\boldsymbol{\alpha\gamma}} p^\nu_{\boldsymbol{\alpha}} o^{\nu'}_{\boldsymbol{\gamma}}\; \chi_{i\boldsymbol{\alpha},i'\boldsymbol{\gamma}}(\boldsymbol{\tau}),$$

with

$$\chi_{i\boldsymbol{\alpha},i'\boldsymbol{\gamma}}(\boldsymbol{\tau}) = \left\langle \mathcal{T}c_{i\alpha}(\tau_1)c^\dagger_{i\alpha'}(\tau_2)c_{i'\gamma}(\tau_3)c^\dagger_{i'\gamma'}(\tau_4)\right\rangle - G_{i\alpha,i\alpha'}(\tau_1,\tau_2)G_{i'\gamma,i'\gamma'}(\tau_3,\tau_4). \tag{11}$$

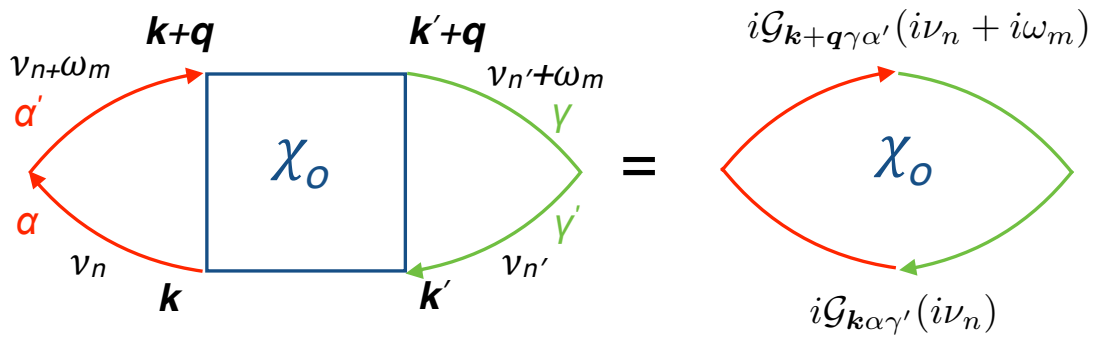

Fig. 9: *Diagram contributing to the linear susceptibility for a non-interacting system. The red lines indicates that the creator/annihilator is originally from the operator $\hat{P}_{\nu'}$ and the green lines indicate that the creator/annihilator is from the operator $\hat{O}_{\nu}$. The corresponding frequencies and momenta are explicitly assigned.*

Performing the Fourier transform from imaginary time to Matsubara frequencies we obtain

$$\chi_{i\boldsymbol{\alpha},i'\boldsymbol{\gamma}}(\boldsymbol{\nu}) = \frac{1}{16}\iiint d\boldsymbol{\tau}\; e^{i\boldsymbol{\nu}\cdot\boldsymbol{\tau}}\chi_{i\boldsymbol{\alpha},i'\boldsymbol{\gamma}}(\boldsymbol{\tau}), \tag{12}$$

where $\boldsymbol{\nu} = (\nu_1, -\nu_2, \nu_3, -\nu_4)$. Due to the conservation of energy, only three of the four ν_i frequencies are independent. Hence, for convenience we set $\nu_1 = \nu_n$, $\nu_2 = \nu_n + \omega_m$, $\nu_3 = \nu_{n'} + \omega_m$, and $\nu_4 = \nu_{n'}$. Next we perform the Fourier transform from site to momentum space. Due to the conservation of lattice momentum, only three of the four $\boldsymbol{k}_i$-vectors are independent. After redefining $\boldsymbol{k}_1 = \boldsymbol{k}$, $\boldsymbol{k}_2 = \boldsymbol{k}+\boldsymbol{q}$, $\boldsymbol{k}_3 = \boldsymbol{k}'+\boldsymbol{q}$ and $\boldsymbol{k}_4 = \boldsymbol{k}'$, we find the expression

$$\chi_{\hat{P}_\nu\,\hat{O}_{\nu'}}(\boldsymbol{q};\boldsymbol{\nu}) = \sum_{\boldsymbol{\alpha}\boldsymbol{\gamma}} p^{\nu}_{\boldsymbol{\alpha}} o^{\nu'}_{\boldsymbol{\gamma}} \sum_{ii'} e^{i(\boldsymbol{T}_i - \boldsymbol{T}_{i'})\cdot\boldsymbol{q}}\chi_{i\boldsymbol{\alpha},i'\boldsymbol{\gamma}}(\boldsymbol{\nu}) = \sum_{\boldsymbol{\alpha}\boldsymbol{\gamma}} p^{\nu}_{\boldsymbol{\alpha}} o^{\nu'}_{\boldsymbol{\gamma}} \underbrace{\frac{1}{N_{\boldsymbol{k}}^2}\sum_{\boldsymbol{k}\boldsymbol{k}'}[\chi(\boldsymbol{q};i\omega_m)]_{\boldsymbol{k}\nu_n\boldsymbol{\alpha},\boldsymbol{k}'\nu_{n'}\boldsymbol{\gamma}}}_{[\chi(\boldsymbol{q};\omega_m)]_{\nu_n\boldsymbol{\alpha},\nu_{n'}\boldsymbol{\gamma}}}.$$

In this expression, by summing over $\boldsymbol{k}$ and $\boldsymbol{k}'$ we obtained $[\chi(\boldsymbol{q};\omega_m)]_{\nu_n\boldsymbol{\alpha},\nu_{n'}\boldsymbol{\gamma}}$. The physical linear response function is given by the sum over the fermionic Matsubara frequencies

$$\chi_{\hat{P}_\nu\,\hat{O}_{\nu'}}(\boldsymbol{q};i\omega_m) = \sum_{\boldsymbol{\alpha}\boldsymbol{\gamma}} p^{\nu}_{\boldsymbol{\alpha}} o^{\nu'}_{\boldsymbol{\gamma}}\,\frac{1}{\beta^2}\sum_{nn'}\Big[\chi(\boldsymbol{q};\omega_m)\Big]_{\nu_n\boldsymbol{\alpha},\nu_{n'}\boldsymbol{\gamma}}. \tag{13}$$

In the case, e.g., of the magnetic susceptibility, the operators $\hat{P}^i_\nu$ and $\hat{O}^{i'}_{\nu'}$ are the three components of the magnetization operator. In the single-orbital limit ($\alpha = \alpha' = \sigma$ and $\gamma = \gamma' = \sigma'$), we thus have, e.g.,

$$o^z_{\boldsymbol{\alpha}} = -g\mu_B\langle\sigma|\hat{\sigma}_z|\sigma\rangle, \qquad p^z_{\boldsymbol{\alpha}} = -g\mu_B\langle\sigma'|\hat{\sigma}_z|\sigma'\rangle.$$

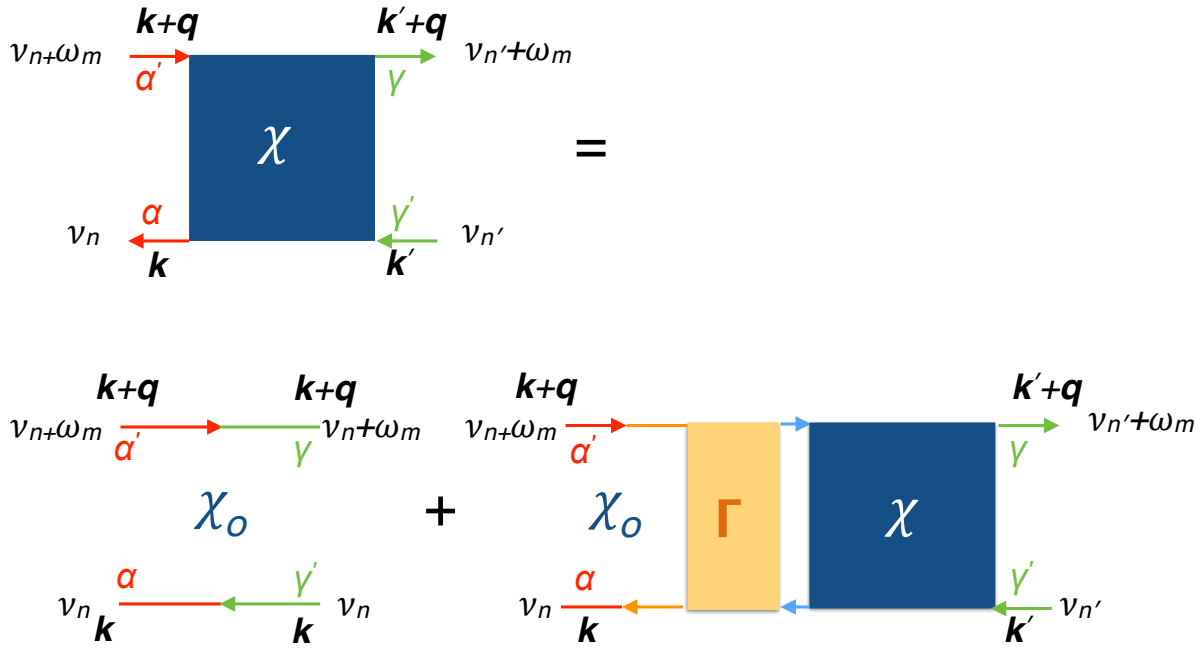

Fig. 10: *Diagrammatic representation of the Bethe-Salpeter equation for the linear susceptibility. The red lines indicates a creator/annihilator stemming from the operator $\hat{P}_\nu$ and the green lines from the operator $\hat{O}_{\nu'}$. The box labeled with Γ is the vertex function, the one labeled with χ the full susceptibility, and χ_0 is the pair-bubble term.*

3.2 DMFT and Bethe-Salpeter equation

To calculate the generalized interacting linear response function introduced in the previous section we can use, in principle, standard many-body perturbation techniques. Let us consider a system described by the multi-band Hubbard model $\hat{H}_0 + \hat{H}_U$, where $\hat{H}_0$ is the non-interacting part. We can formally construct a perturbation series for $\chi_{\hat{P}_\nu \hat{O}_{\nu'}}(\boldsymbol{q}; i\omega_m)$ in the interaction $\hat{H}_U$. The zero-order contribution is the linear response function for $\hat{H}_0$. Thus, due to Wick's theorem

$$\Big[\chi_0(\boldsymbol{q}; i\omega_m)\Big]_{\nu_n \boldsymbol{\alpha}, \nu_{n'} \boldsymbol{\gamma}} = \frac{1}{N_{\boldsymbol{k}}^2} \sum_{\boldsymbol{k}\boldsymbol{k}'} \underbrace{\Big[-\beta N_{\boldsymbol{k}} \mathcal{G}_{\boldsymbol{k}\alpha\gamma'}(i\nu_n)\, \mathcal{G}_{\boldsymbol{k}'+\boldsymbol{q}\alpha'\gamma}(i\nu_{n'}+i\omega_m)\, \delta_{n,n'} \delta_{\boldsymbol{k},\boldsymbol{k}'} \Big]}_{\Big[\chi_0(\boldsymbol{q};i\omega_m)\Big]_{\boldsymbol{k}\nu_n\boldsymbol{\alpha},\boldsymbol{k}'\nu_{n'}\boldsymbol{\gamma}}} . \quad (14)$$

The Feynman diagram corresponding to $[\chi_0(\boldsymbol{q}; \omega_m)]_{\boldsymbol{k}\nu_n\boldsymbol{\alpha},\boldsymbol{k}'\nu_{n'}\boldsymbol{\gamma}}$ is shown in Fig. 9. Once we switch-on the interaction, many-body perturbation theory leads to the Bethe-Salpeter (BS) equation, pictorially shown in Fig. 10. The susceptibility can then be expressed as follows

$$\Big[\chi(\boldsymbol{q}; i\omega_m)\Big]_{\nu_n \boldsymbol{\alpha}, \nu_{n'} \boldsymbol{\gamma}} = \frac{1}{N_{\boldsymbol{k}}^2} \sum_{\boldsymbol{k}\boldsymbol{k}'} \Big[\chi_0(\boldsymbol{q}; i\omega_m) + \frac{1}{N_{\boldsymbol{k}}^2} \chi_0(\boldsymbol{q}; i\omega_m) \Gamma(\boldsymbol{q}; i\omega_m) \chi(\boldsymbol{q}; i\omega_m)\Big]_{\boldsymbol{k}\nu_n\boldsymbol{\alpha},\nu_{n'}\boldsymbol{k}'\boldsymbol{\gamma}} .$$

For systems for which the dynamical mean-field is a good approximation, however, it is more convenient to construct a diagrammatic series starting from the DMFT linear response function

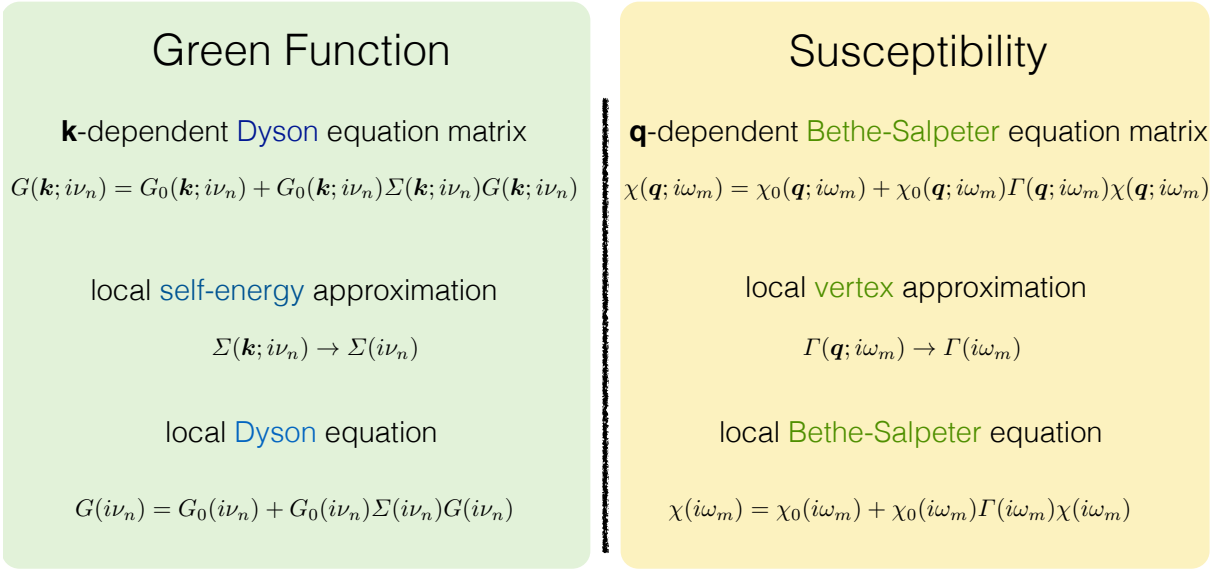

Fig. 11: *Analogies between the calculation of the Green function $G(\boldsymbol{k};i\nu_n)$ in the local-self-energy approximation (left) and the calculation of the response function $\chi(\boldsymbol{q};i\omega_m)$ in the local vertex approximation (right). Each term in the general Bethe-Salpeter equation can be viewed as a square matrix of dimension $N_{\boldsymbol{k}}N_nN_\alpha$, where $N_{\boldsymbol{k}}$ is the number of $\boldsymbol{k}$ points, N_n the number of fermionic Matsubara frequencies, N_α the number of flavors.*

rather than from the non-interacting term. If we do so, $\chi_0(\boldsymbol{q};\omega_m)$ is still given by Eq. (14), but with $\mathcal{G}$ replaced by the DMFT Green function matrices. Hence

$$[\chi_0(\boldsymbol{q};i\omega_m)]_{\nu_n\boldsymbol{\alpha},\nu_{n'}\boldsymbol{\gamma}} = -\beta\delta_{nn'}\frac{1}{N_{\boldsymbol{k}}}\sum_{\boldsymbol{k}} G_{\alpha\gamma'}(\boldsymbol{k};i\nu_n)\, G_{\alpha'\gamma}(\boldsymbol{k}+\boldsymbol{q};i\nu_n+i\omega_m).$$

There is, however, a catch: the vertex $\Gamma(\boldsymbol{q};i\omega_m)$ is unknown. In the infinite dimension limit it has been shown that the vertex can be replaced by a local quantity [4, 14]. Assuming that, in the spirit of the dynamical mean-field approximation, for a real 3-dimensional system we can do the same, we set

$$\Gamma(\boldsymbol{q};i\omega_m) \longrightarrow \Gamma(i\omega_m).$$

Thus, dropping for simplicity the flavor indices, after performing the $\boldsymbol{k}$ sums, the Bethe-Salpeter equation becomes

$$\chi(\boldsymbol{q};i\omega_m) = \chi_0(\boldsymbol{q};i\omega_m) + \chi_0(\boldsymbol{q};i\omega_m)\Gamma(i\omega_m)\chi(\boldsymbol{q};i\omega_m).$$

By solving it we find, formally

$$\chi^{-1}(\boldsymbol{q};i\omega_m) = \chi_0^{-1}(\boldsymbol{q};i\omega_m) - \Gamma(i\omega_m). \tag{15}$$

To actually obtain $\chi(\boldsymbol{q};i\omega_m)$ from this equation we need to calculate first the local vertex. The latter can be obtained using a further approximation, i.e., assuming that (15) is also satisfied if

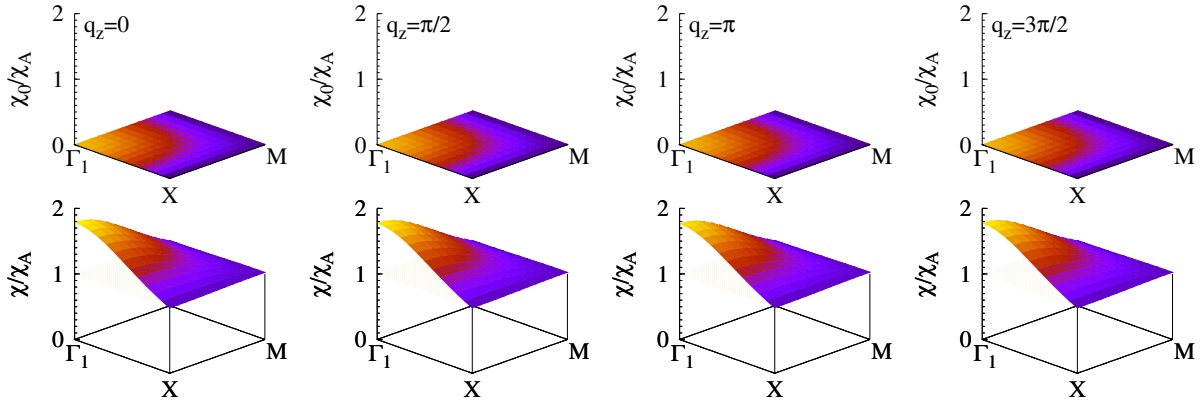

Fig. 12: *$VOMoO_4$: Static magnetic susceptibility $\chi(\mathbf{q};0)/\chi_A(0)$ in the q_x, q_y plane for representative q_z values, $T \sim 380$ K and $U = 5$ eV. The normalization $\chi_A(0) \sim \mu^2_{\rm eff}/k_BT$ is the atomic susceptibility in the large βU limit. Top panels: $\Gamma = 0$. Bottom panels: $\Gamma \neq 0$. Special points: $\Gamma_1 = (2\pi, 0)$, X$= (\pi, 0)$ and M$= (\pi, \pi)$. Rearranged from Ref. [11].*

we replace the $\boldsymbol{q}$-dependent susceptibilities with their local counterparts, defined as

$$\chi_0(i\omega_m) = \frac{1}{N_{\boldsymbol{q}}} \sum_{\boldsymbol{q}} \chi_0(\boldsymbol{q}; i\omega_m),$$
$$\chi(i\omega_m) = \frac{1}{N_{\boldsymbol{q}}} \sum_{\boldsymbol{q}} \chi(\boldsymbol{q}; i\omega_m).$$

The first term is calculated directly from the DMFT Green function $\chi_0(\boldsymbol{q}; i\omega_m)$. The second term, $\chi(i\omega_m)$, is obtained via the quantum-impurity solver in the final iteration of the DMFT self-consistency loop. By inverting the local BS equation we have

$$\Gamma(i\omega_m) = \chi_0^{-1}(i\omega_m) - \chi^{-1}(i\omega_m). \tag{16}$$

Replacing $\Gamma(i\omega_m)$ into Eq. (15) yields the $\boldsymbol{q}$-dependent susceptibility. It has to be noticed that, although the two equations (15) and (16) look innocent, solving them numerically is a delicate task because the local susceptibility is in general not diagonal in n, n' and does not decay very fast with the frequencies. There are, however, various ways to reduce the computational costs, e.g., via extrapolations [11] or using compact representations based on auxiliary polynomials [15, 16]. The method just illustrated for the calculation of linear response functions in the local vertex approximation bears resemblance with the approach adopted for the calculation of the Green functions in the local self-energy approximation. These analogies are schematically pointed out in Fig. 11. Instead, in Fig. 12 we show as an example the case of the static magnetic susceptibility for a one-band system, the $S = 1/2$ frustrated Mott insulator $VOMoO_4$. The figure shows both the "bubble" term $\chi_0(\boldsymbol{q}; i\omega_m)$ (top panels) and the full susceptibility $\chi(\boldsymbol{q}; i\omega_m)$ (bottom panels). The two differ sizably in absolute value. In addition, as we will discuss later, the $\chi_0(\boldsymbol{q}; i\omega_m)$ term alone is very weakly dependent on the temperature. The expected Curie-Weiss-like behavior is only recovered when $\Gamma(i\omega_m)$ is taken into account.

3.3 The local susceptibility: Legendre representation

The core of the approach described in the previous section is the calculation of the local susceptibility tensor, $\chi_{\boldsymbol{\alpha\gamma}}(\boldsymbol{\tau})$. In DMFT all local observables $\langle\hat{O}\rangle$ are obtained via the quantum-impurity solver, for example the continuous-time hybridization expansion QMC technique presented in Section 2.3. Susceptibilities, however, require sizably longer computational time than Green-function matrices. Thus, instead of calculating directly $\chi_{\boldsymbol{\alpha\gamma}}(\boldsymbol{\tau})$, it is convenient to express the tensor elements in a basis of orthogonal functions $f_l^m(\tau)$, chosen such that the representation is as compact as possible. A successful choice [15, 16] is

$$f_l^m(\tau) = e^{-i\phi_m(\tau)} \begin{cases} \sqrt{2l+1}\; p_l(x(\tau)), & \tau > 0 \\ -(-1)^m\sqrt{2l+1}\; p_l(x(\tau+\beta)), & \tau < 0 \end{cases}$$

where $p_l(x(\tau))$ is a Legendre polynomial of degree l, with $x(\tau) = 2\tau/\beta - 1$; here the factor $(-1)^m$ in the second row ensures anti-periodicity for all values of m, which is the index for the bosonic Matsubara frequency ω_m. Via the orthogonality properties of the polynomials we obtain

$$\chi_{\boldsymbol{\alpha\gamma}}(i\omega_m) = \frac{1}{\beta^2}\sum_{ll'} f_l^{-m}(0^+)\; \chi^{l,l'}_{\boldsymbol{\alpha\gamma}}(i\omega_m)\; f_{l'}^{-m}(0^+). \tag{17}$$

The expansion coefficients in Eq. (17) take the form

$$\chi^{l,l'}_{\boldsymbol{\alpha\gamma}}(i\omega_m) = \int_0^\beta d\tau_{23}\int_0^\beta d\tau_{12}\int_0^\beta d\tau_{34}\; e^{-i\omega_m\tau_{23}} f_l^m(\tau_{12})\chi^{\alpha\alpha'}_{\gamma\gamma'}(\tau_{14},\tau_{24},\tau_{34},0) f_{l'}^m(\tau_{34}), \tag{18}$$

where $\tau_{ij} = \tau_i - \tau_j$, with $\tau_{14} = \tau_{12}+\tau_{23}+\tau_{34}$, and $\tau_{24} = \tau_{23}+\tau_{34}$. The phase defining the gauge is $\phi_m(\tau) = \omega_m\tau/2$ and does not depend on l. As we have seen, in quantum Monte Carlo the observables are obtained as the average over the visited configurations c. Splitting (18) into two terms [16] we have

$$\left\langle \chi^{l,l'}_{\boldsymbol{\alpha\gamma}}(i\omega_m)\right\rangle_c = \left\langle \mathcal{C}^{l,l'}_{\boldsymbol{\alpha\gamma}}(i\omega_m)\right\rangle_c - \beta\delta_{m,0}\left\langle G^l_{\boldsymbol{\alpha}}\right\rangle_c\left\langle G^{l'}_{\boldsymbol{\gamma}}\right\rangle_c.$$

The first term can be expressed as

$$\left\langle C^{l,l'}_{\boldsymbol{\alpha\gamma}}(i\omega_m)\right\rangle_c = \frac{1}{\beta}\sum_{bb'dd'}^{N_B}\sum_{i,j}^{k_b,k_d}\sum_{i',j'}^{k_{b'},k_{d'}} f_l^m(\tau_{dj}-\bar\tau_{bi}) f_{l'}^m(\tau_{d'j'}-\bar\tau_{b'i'}) c^{db,d'b'}_{ji,j'i'}(i\omega_m)\delta_{\boldsymbol{\alpha},(\alpha_{dj},\bar\alpha_{bi})}\delta_{\boldsymbol{\gamma},(\alpha_{d'j'},\bar\alpha_{b'i'})}$$

where

$$c^{db,d'b'}_{ji,j'i'}(i\omega_m) = (w^{db}_{ji}w^{d'b'}_{j'i'} - w^{d'b}_{j'i}w^{db'}_{ji'})\, e^{-i\omega_m(\bar\tau_{bi}-\tau_{d'j'})}.$$

Here the imaginary times τ_{bi} and $\bar\tau_{bi}$ all vary in the interval $[0,\beta)$. The letters b and d label the N_B flavors decoupled by symmetry, e.g., $\{\uparrow,\downarrow\}$. Finally, $w^{db}_{ji} = \delta_{b,d}\mathcal{M}^{k_b}_{bj,bi}$, where the matrix $\mathcal{M}^{k_b} = [\mathcal{F}_0^{k_b}]^{-1}$ is the inverse of the hybridization function matrix $\mathcal{F}_0^{k_b}$ for expansion order k_b. The Green functions in the second term are instead given by

$$\left\langle G^l_{\boldsymbol{\alpha}}\right\rangle_c = -\frac{1}{\beta}\sum_{b}^{N_B}\sum_{ij}^{k_b} f_l^0(\tau_{bj}-\bar\tau_{bi})\, w^{bb}_{ji}\,\delta_{\boldsymbol{\alpha},(\alpha_{bj},\bar\alpha_{bi})}.$$

3.4 Magnetic susceptibility for the single-band Hubbard model

The magnetic susceptibility is the linear response to an external magnetic field. The associated site susceptibility is

$$\chi^{i,i'}_{zz}(\boldsymbol{\tau}) = \left\langle \mathcal{T}\hat{M}^i_z(\tau)\hat{M}^{i'}_z(0)\right\rangle_0 - \left\langle \hat{M}^i_z\right\rangle_0\left\langle \hat{M}^{i'}_z\right\rangle_0,$$

where $\hat{M}^i_z = -g\mu_B\hat{S}^i_z$ is the magnetization for lattice site i. Its Fourier transform is

$$\begin{aligned}\chi_{zz}(\boldsymbol{q}; i\omega_m) &= \sum_{ii'} e^{i\boldsymbol{q}\cdot(\boldsymbol{T}_i-\boldsymbol{T}_{i'})}\int d\tau\; e^{i\omega_m\tau}\chi^{i,i'}_{zz}(\tau)\\ &= \left\langle \hat{M}_z(\boldsymbol{q};\omega_m)\hat{M}_z(-\boldsymbol{q};0)\right\rangle_0 - \left\langle \hat{M}_z(\boldsymbol{q})\right\rangle_0\left\langle \hat{M}_z(-\boldsymbol{q})\right\rangle_0, \end{aligned} \tag{19}$$

where ω_m is a bosonic Matsubara frequency. For the one-band Hubbard model, the magnetization operator can be expressed in the basis of Bloch functions as

$$\hat{M}_z(\boldsymbol{q}) = -\frac{g\mu_B}{2}\sum_{\boldsymbol{k}}\sum_{\sigma}\sigma c^\dagger_{\boldsymbol{k}+\boldsymbol{q}\sigma}c_{\boldsymbol{k}\sigma}, \tag{20}$$

where $\sigma = 1$ for spin up and $\sigma = -1$ for spin down. To obtain the magnetic response function we thus have to calculate the imaginary-time tensor with elements

$$\begin{aligned}\left[\chi(\boldsymbol{q};\boldsymbol{\tau})\right]_{\boldsymbol{k}\sigma,\boldsymbol{k}'\sigma'} &= \left\langle \mathcal{T}c_{\boldsymbol{k}\sigma}(\tau_1)c^\dagger_{\boldsymbol{k}+\boldsymbol{q}\sigma}(\tau_2)c_{\boldsymbol{k}'+\boldsymbol{q}\sigma'}(\tau_3)c^\dagger_{\boldsymbol{k}'\sigma'}(\tau_4)\right\rangle_0\\ &\quad - \left\langle \mathcal{T}c_{\boldsymbol{k}\sigma}(\tau_1)c^\dagger_{\boldsymbol{k}+\boldsymbol{q}\sigma}(\tau_2)\right\rangle_0\left\langle \mathcal{T}c_{\boldsymbol{k}'+\boldsymbol{q}\sigma'}(\tau_3)c^\dagger_{\boldsymbol{k}'\sigma'}(\tau_4)\right\rangle_0. \end{aligned} \tag{21}$$

The associated imaginary-time magnetic susceptibility is then given by

$$\chi_{zz}(\boldsymbol{q};\boldsymbol{\tau}) = (g\mu_B)^2\frac{1}{4}\sum_{\sigma\sigma'}\sigma\sigma'\underbrace{\frac{1}{\beta}\frac{1}{N^2_{\boldsymbol{k}}}\sum_{\boldsymbol{k}\boldsymbol{k}'}\left[\chi(\boldsymbol{q};\boldsymbol{\tau})\right]_{\boldsymbol{k}\sigma,\boldsymbol{k}'\sigma'}}_{\chi_{\sigma\sigma\sigma'\sigma'}(\boldsymbol{q};\boldsymbol{\tau})}. \tag{22}$$

After we Fourier transform with respect to imaginary time and sum over the fermionic Matsubara frequencies, we have

$$\chi_{zz}(\boldsymbol{q}; i\omega_m) = (g\mu_B)^2\frac{1}{4}\sum_{\sigma\sigma'}\sigma\sigma'\frac{1}{\beta^2}\sum_{nn'}\chi^{n,n'}_{\sigma\sigma\sigma'\sigma'}(\boldsymbol{q}; i\omega_m), \tag{23}$$

where

$$\chi^{n,n'}_{\sigma\sigma\sigma'\sigma'}(\boldsymbol{q}; i\omega_m) = \frac{1}{16}\iiint d\boldsymbol{\tau}\; e^{i\boldsymbol{\nu}\cdot\boldsymbol{\tau}}\chi_{\sigma\sigma\sigma'\sigma'}(\boldsymbol{q};\boldsymbol{\tau}). \tag{24}$$

For $\omega_n = 0$ we obtain the static magnetic susceptibility.

3.4.1 Non-interacting limit

In the non-interacting limit we can use Wick's theorem to simplify Eq. (21). It follows that the elements of the two-particle Green function tensor vanish if $\boldsymbol{k} \neq \boldsymbol{k}'$. In the paramagnetic case, Eq. (22) then becomes

$$\chi_{zz}(\boldsymbol{q};\boldsymbol{\tau}) = -(g\mu_B)^2 \frac{1}{4}\frac{1}{\beta}\frac{1}{N_{\boldsymbol{k}}}\sum_{\boldsymbol{k}}\sum_{\sigma}\mathcal{G}_{\boldsymbol{k}\sigma}(\tau_{14})\mathcal{G}_{\boldsymbol{k}+\boldsymbol{q}\sigma}(-\tau_{23}).$$

For the frequency-dependent magnetic susceptibility Eq. (23) we have instead

$$\chi_{zz}(\boldsymbol{q};i\omega_m) = (g\mu_B)^2 \frac{1}{4}\frac{1}{\beta^2}\sum_{nn'}\sum_{\sigma}\chi^{n,n'}_{\sigma\sigma\sigma\sigma}(\boldsymbol{q};i\omega_m),$$

where

$$\sum_{\sigma}\chi^{n,n'}_{\sigma\sigma\sigma\sigma}(\boldsymbol{q};i\omega_m) = -\beta\frac{1}{N_{\boldsymbol{k}}}\sum_{\boldsymbol{k}}\sum_{\sigma}\mathcal{G}_{\boldsymbol{k}\sigma}(i\nu_n)\,\mathcal{G}_{\boldsymbol{k}+\boldsymbol{q}\sigma}(i\nu_n+i\omega_m)\,\delta_{n,n'}. \tag{25}$$

The actual dynamical susceptibility is then given by

$$\chi_{zz}(\boldsymbol{q};i\omega_m) = -\,(g\mu_B)^2\,\frac{1}{4}\frac{1}{N_{\boldsymbol{k}}}\sum_{\boldsymbol{k}}\sum_{\sigma}\frac{n_\sigma(\varepsilon_{\boldsymbol{k}+\boldsymbol{q}}) - n_\sigma(\varepsilon_{\boldsymbol{k}})}{\varepsilon_{\boldsymbol{k}+\boldsymbol{q}} - \varepsilon_{\boldsymbol{k}} + i\omega_m}.$$

In the $\boldsymbol{q}\to 0$ and $T\to 0$ limit, setting $\omega_m = 0$ we recover the static Pauli susceptibility

$$\chi_{zz}(\boldsymbol{0};0) = \frac{1}{4}\,(g\mu_B)^2\,\rho(\varepsilon_F),$$

$$\rho(\varepsilon_F) = -\sum_{\sigma}\frac{1}{N_{\boldsymbol{k}}}\sum_{\boldsymbol{k}}\left.\frac{dn_\sigma(\varepsilon_{\boldsymbol{k}})}{d\varepsilon_{\boldsymbol{k}}}\right|_{T=0}.$$

Figure 13 shows (at half filling) the non-interacting spin susceptibility in the x-y plane for a d-dimensional hypercubic lattice with dispersion

$$\varepsilon_{\boldsymbol{k}} = -2t\sum_{n=1}^{d}\cos k_d.$$

In $d = 1$ and for $T\to 0$, $\chi_{zz}(\boldsymbol{q};0)$ diverges at the antiferromagnetic vector $\boldsymbol{q}_C = (\pi/a, 0, 0)$; in two dimensions this happens at $\boldsymbol{q}_C$=$(\pi/a, \pi/a, 0)$; in three dimensions at $\boldsymbol{q}_C$=$(\pi/a, \pi/a, \pi/a)$, not shown in the figure. These are perfect nesting vectors, for which

$$\varepsilon_{\boldsymbol{k}+\boldsymbol{q}_C} = -\varepsilon_{\boldsymbol{k}},$$

so that

$$\chi_0(\boldsymbol{q}_C;0) \propto \frac{1}{4}\int_{-\infty}^{\varepsilon_F} d\varepsilon\,\frac{\rho(\varepsilon)}{\varepsilon}.$$

Under these conditions an arbitrarily small U can cause a magnetic transition with magnetic vector $\boldsymbol{q}_C$, e.g., via a Stoner-like mechanism.

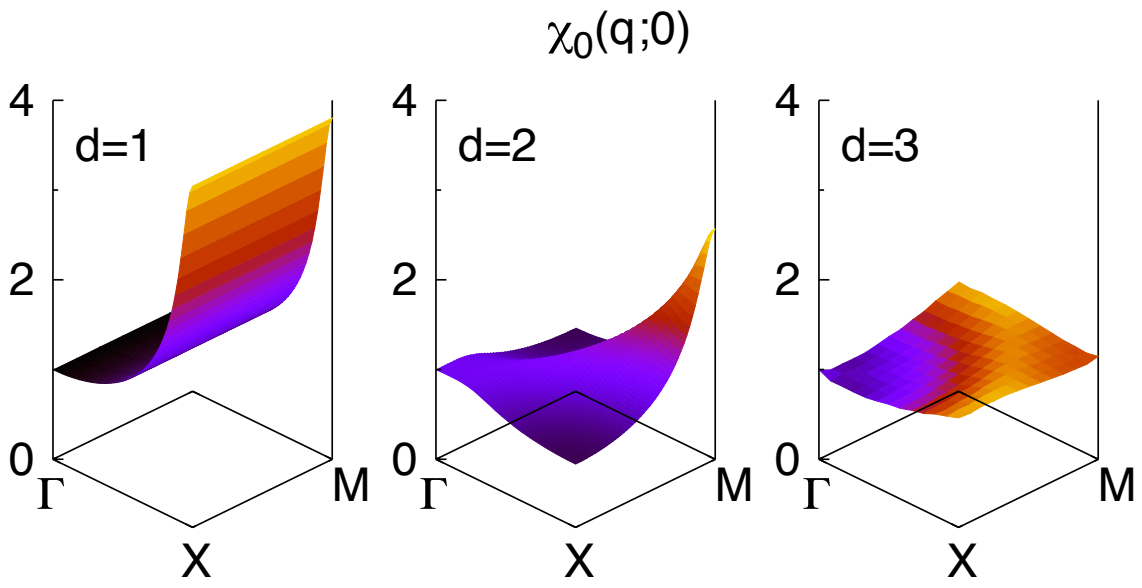

Fig. 13: *The ratio $\chi_0(\boldsymbol{q};0)/\chi_0(\boldsymbol{0};0)$ in the x-y plane for a hypercubic lattice with $t = 0.4$ eV ($T \sim 230$ K) at half filling. From left to right: one, two, and three dimensions.*

3.4.2 Atomic limit

Let us now consider the opposite extreme, the atomic limit. First we adopt a simple approach, i.e., we directly calculate the right-hand side of Eq. (19) by summing up the contributions of the atomic states, $|0\rangle$, $c^\dagger_\uparrow|0\rangle$, $c^\dagger_\downarrow|0\rangle$, $c^\dagger_\uparrow c^\dagger_\downarrow|0\rangle$; since all atoms are decoupled, only on-site terms $i = i'$ contribute. At half filling we thus have

$$\chi_{zz}(\boldsymbol{q}; i\omega_m) = (g\mu_B)^2 \frac{1}{4k_BT} \frac{e^{\beta U/2}}{1+e^{\beta U/2}} \delta_{\omega_m,0}. \tag{26}$$

The same expression can be obtained following the general procedure outlined in the previous pages, i.e., starting from the two-particle Green function tensor $\chi_{\sigma\sigma\sigma'\sigma'}(\boldsymbol{q};\boldsymbol{\tau})$, defined in Eq. (22) for the single-band Hubbard model. In the atomic limit, it is convenient to work in real space, since

$$\chi_{\sigma\sigma\sigma'\sigma'}(\boldsymbol{q};\boldsymbol{\tau}) = \frac{1}{\beta} \sum_i \chi_{i\sigma\sigma,i\sigma'\sigma'}(\boldsymbol{\tau}).$$

Thanks to the symmetries of the tensor in imaginary time, it is sufficient to calculate $\chi_{i\sigma\sigma,i\sigma'\sigma'}(\boldsymbol{\tau})$ for positive times $0 < \tau_{j4} < \beta$, where $\tau_{j4} = \tau_j - \tau_4$ with $j = 1, 2, 3$. Due to the time ordering operator we have, however, to consider separately six different imaginary-time sectors. In the Appendix one can find a list of all these sectors and their contributions. For simplicity, we discuss here explicitly only the case $\tau_{14} > \tau_{24} > \tau_{34} > 0$ and label the corresponding $\boldsymbol{\tau}$-vector as $\boldsymbol{\tau}^+$. Calculating the trace we obtain

$$\chi_{i\sigma\sigma,i\sigma'\sigma'}(\boldsymbol{\tau}^+) = \frac{e^{\tau_{12}U/2+\tau_{34}U/2} + \delta_{\sigma\sigma'} e^{(\beta-\tau_{12})U/2-\tau_{34}U/2}}{2(1+e^{\beta U/2})} - G^\sigma_{i,i}(\tau_{12})\, G^{\sigma'}_{i,i}(\tau_{34}).$$

In the paramagnetic case the mean-field terms $G^{\sigma}_{i,i}(\tau_{12})\,G^{\sigma'}_{i,i}(\tau_{34})$ cancel out in the actual magnetic linear response function, so here we do not give their form explicitly. For a single atom, the contribution of the $\boldsymbol{\tau}^+$ sector to the imaginary-time magnetic susceptibility is

$$\chi_{zz}(\boldsymbol{\tau}^+) = (g\mu_B)^2\,\frac{1}{4}\frac{1}{\beta}\sum_{\sigma\sigma'}\sigma\sigma'\chi_{i\sigma\sigma,i\sigma'\sigma'}(\boldsymbol{\tau}^+) = \frac{(g\mu_B)^2}{4\beta}\frac{1}{(1+e^{\beta U/2})}e^{(\beta-\tau_{12}-\tau_{34})U/2}.$$

Summing up the contributions of all imaginary-time sectors and performing the Fourier transform we obtain $\chi^{n,n'}_{\sigma\sigma\sigma'\sigma'}(i\omega_n)$, defined in Eq. (24). For $U \neq 0$ this tensor is non-diagonal in the fermionic Matsubara frequencies. For $\omega_n = 0$ we have [11]

$$\begin{aligned}\sum_{\sigma\sigma'}\sigma\sigma'\,\chi^{n,n'}_{i\sigma\sigma,i\sigma'\sigma'}(0) =& M_{n'}\frac{dM_n}{dy} + M_n\frac{dM_{n'}}{dy} - \beta n(y)\left[\delta_{n,n'}+\delta_{n,-n'}\right]\frac{dM_n}{dy} + \beta n(-y)M_nM_{n'} \\ &-\frac{1}{y}\left\{M_{n'} - \beta\left[n(y)\delta_{n,-n'} - n(-y)\delta_{n,n'}\right]\right\}M_n \end{aligned} \tag{27}$$

where

$$M_n = \frac{1}{i\nu_n - y} - \frac{1}{i\nu_n + y}. \tag{28}$$

We can now calculate the magnetic susceptibility via Eq. (23), recovering the expected result, Eq. (26). The resulting atomic magnetic susceptibility is thus proportional to $1/k_BT$, i.e., has a Curie-like behavior; furthermore it is zero at finite frequency. The temperature dependence can be remarkably different from the $U = 0$ limit. Indeed, if the density of states is flat around the Fermi level, as it is often the case in three-dimensional lattices, the non-interacting Pauli susceptibility $\chi_{zz}(\mathbf{0};0)$ is weakly temperature dependent. A strong temperature dependence can be found, however, if, e.g., a logarithmic van-Hove singularity is at the Fermi level, as in the example discussed in the previous subsection for the square lattice at half filling.

3.4.3 DMFT: $\chi_0(\mathrm{q};\omega)$ and the Bethe-Salpeter equation

In order to calculate the magnetic susceptibility with DMFT, we first need $\chi_0(\mathbf{q};\omega)$. Here for simplicity we consider only the two-dimensional case with $\varepsilon_{\boldsymbol{k}} = -2t(\cos k_x + \cos k_y)$. In the atomic limit we can rewrite the local Green function as

$$G^{\sigma}_{i,i}(i\nu_n) = \frac{1}{i\nu_n + \mu - \varepsilon_d - \Sigma^{\sigma}_l(i\nu_n)},$$

where the local self-energy is given by

$$\Sigma^{\sigma}_l(i\nu_n) = \frac{U}{2} + \frac{U^2}{4}\frac{1}{i\nu_n + \mu - \varepsilon_d - \frac{U}{2}}, \tag{29}$$

and $\mu = \varepsilon_d + \frac{U}{2}$ at half filling. In the Mott insulating regime, i.e., for small but finite t/U, we can assume that the local self-energy has the same form (29), with $U^2/4$ replaced by a quantity which plays the role of a dimensionless *order parameter* [17] for the insulating phase

$$\frac{1}{r_U}\frac{4}{U^2} = \int_{-\infty}^{+\infty} d\varepsilon\,\frac{\rho(\varepsilon)}{\varepsilon^2}. \tag{30}$$

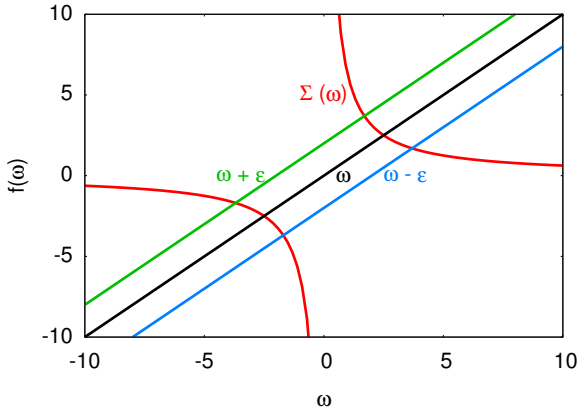

Fig. 14: *Graphical solution of the equation* $\omega - \varepsilon_{\boldsymbol{k}} = \Sigma_l^\sigma(\omega)$ *yielding the poles* $E_{\boldsymbol{k}}^+$ *and* $E_{\boldsymbol{k}}^-$ *of the Green function defined in Eq. (31).*

Here $\rho(\varepsilon)$ is the density of states per spin. The integral in Eq. (30) diverges in the metallic phase. The Green function can then be rewritten as

$$G_{\sigma\sigma}(\boldsymbol{k}; i\nu_n) = \frac{1}{i\nu_n - \Sigma_l^\sigma(i\nu_n) - \varepsilon_{\boldsymbol{k}}} = \frac{1}{E_{\boldsymbol{k}}^+ - E_{\boldsymbol{k}}^-}\left[\frac{E_{\boldsymbol{k}}^+}{i\nu_n - E_{\boldsymbol{k}}^+} - \frac{E_{\boldsymbol{k}}^-}{i\nu_n - E_{\boldsymbol{k}}^-}\right] \tag{31}$$

where $E_{\boldsymbol{k}}^+$ and $E_{\boldsymbol{k}}^-$ are the two roots of the equation $\omega - \Sigma_l^\sigma(\omega) - \varepsilon_{\boldsymbol{k}} = 0$,

$$E_{\boldsymbol{k}}^\pm = \frac{1}{2}\varepsilon_{\boldsymbol{k}} \pm \frac{1}{2}\sqrt{\varepsilon_{\boldsymbol{k}}^2 + r_U\, U^2}.$$

By performing the Matsubara sums, one finds

$$\begin{aligned}\chi_{zz}^0(\boldsymbol{q}; 0) &= (g\mu_B)^2 \frac{1}{4}\sum_\sigma \frac{1}{\beta^2}\sum_n \chi_{\sigma\sigma\sigma\sigma}^{n,n}(0) \\ &= (g\mu_B)^2 \frac{1}{2}\frac{1}{N_{\boldsymbol{k}}}\sum_{\boldsymbol{k}}\Big[\underbrace{-I_{\boldsymbol{k},\boldsymbol{q}}^{++} - I_{\boldsymbol{k},\boldsymbol{q}}^{--}}_{A_{\boldsymbol{k},\boldsymbol{q}}} + \underbrace{I_{\boldsymbol{k},\boldsymbol{q}}^{+-} + I_{\boldsymbol{k},\boldsymbol{q}}^{-+}}_{B_{\boldsymbol{k},\boldsymbol{q}}},\Big]\end{aligned}$$

where, setting $\alpha = \pm$ and $\gamma = \pm$,

$$I_{\boldsymbol{k},\boldsymbol{q}}^{\alpha\gamma} = \frac{E_{\boldsymbol{k}}^\alpha\, E_{\boldsymbol{k}+\boldsymbol{q}}^\gamma}{\big(E_{\boldsymbol{k}}^+ - E_{\boldsymbol{k}}^-\big)\big(E_{\boldsymbol{k}+\boldsymbol{q}}^+ - E_{\boldsymbol{k}+\boldsymbol{q}}^-\big)}\frac{n(E_{\boldsymbol{k}}^\alpha) - n(E_{\boldsymbol{k}+\boldsymbol{q}}^\gamma)}{E_{\boldsymbol{k}}^\alpha - E_{\boldsymbol{k}+\boldsymbol{q}}^\gamma}.$$

In the $\boldsymbol{q} \to \boldsymbol{0}$ limit

$$\begin{aligned}A_{\boldsymbol{k},\boldsymbol{0}} &= \beta\,\left[\frac{(E_{\boldsymbol{k}}^+)^2}{\varepsilon_{\boldsymbol{k}}^2 + r_U\, U^2}\, n(E_{\boldsymbol{k}}^+)\big(1 - n(E_{\boldsymbol{k}}^+)\big) + \frac{(E_{\boldsymbol{k}}^-)^2}{\varepsilon_{\boldsymbol{k}}^2 + r_U\, U^2}\, n(E_{\boldsymbol{k}}^-)\big(1 - n(E_{\boldsymbol{k}}^-)\big)\right] \\ B_{\boldsymbol{k},\boldsymbol{0}} &= \frac{r_U\, U^2}{2(\varepsilon_{\boldsymbol{k}}^2 + r_U\, U^2)^{3/2}}\left(n(E_{\boldsymbol{k}}^-) - n(E_{\boldsymbol{k}}^+)\right).\end{aligned}$$

In the large βU limit, the $A_{\boldsymbol{k},\boldsymbol{0}}$ term, proportional to the density of states at the Fermi level, vanishes exponentially; the $B_{\boldsymbol{k},\boldsymbol{0}}$ term yields the dominant contribution. Hence

$$\chi_{zz}^0(\boldsymbol{0}; 0) \sim (g\mu_B)^2 \frac{1}{4}\frac{1}{N_{\boldsymbol{k}}}\sum_{\boldsymbol{k}} \frac{r_U\, U^2}{(\varepsilon_{\boldsymbol{k}}^2 + r_U\, U^2)^{3/2}} \sim (g\mu_B)^2 \frac{1}{4\sqrt{r_U}\, U}\left[1 - \frac{3}{2}\frac{1}{N_{\boldsymbol{k}}}\sum_{\boldsymbol{k}} \frac{\varepsilon_{\boldsymbol{k}}^2}{r_U\, U^2} + \dots\right].$$

The right-hand side is equal to the atomic term $\chi^0_{zz}(0)$ minus a correction of order t^2/U^3. As we can see, $\chi^0_{zz}(\mathbf{0};0)$ is small and weakly dependent on the temperature. In the Mott-insulating regime, due to the superexchange interaction, the two-dimensional Hubbard model exhibits an antiferromagnetic instability at $\boldsymbol{q}_C = (\pi/a, \pi/a, 0)$. Let us then calculate $\chi^0_{zz}(\boldsymbol{q}_C;0)$ and compare it with $\chi^0_{zz}(\mathbf{0};0)$. Since, as we have seen, $\varepsilon_{\boldsymbol{k}+\boldsymbol{q}_C} = -\varepsilon_{\boldsymbol{k}}$, we find

$$A_{\boldsymbol{k},\boldsymbol{q}_C} = \frac{1}{2}\frac{r_U\,U^2}{\varepsilon^2_{\boldsymbol{k}} + r_U\,U^2}\frac{n(E^+_{\boldsymbol{k}}-\varepsilon_{\boldsymbol{k}}) - n(E^+_{\boldsymbol{k}})}{\varepsilon_{\boldsymbol{k}}}$$

$$B_{\boldsymbol{k},\boldsymbol{q}_C} = \frac{1}{2}\frac{\varepsilon^2_{\boldsymbol{k}}}{\varepsilon^2_{\boldsymbol{k}} + r_U\,U^2}\frac{n(E^+_{\boldsymbol{k}}-\varepsilon_{\boldsymbol{k}}) - n(E^+_{\boldsymbol{k}})}{\varepsilon_{\boldsymbol{k}}} - \frac{1}{2}\frac{1}{\sqrt{\varepsilon^2_{\boldsymbol{k}} + r_U\,U^2}}\left(n(E^+_{\boldsymbol{k}}) - n(E^-_{\boldsymbol{k}})\right),$$

and therefore

$$\chi_0(\boldsymbol{q}_C;0) \sim (g\mu_B)^2\frac{1}{4\sqrt{r_U}U}\left(1 - \frac{1}{2}\frac{1}{N_{\boldsymbol{k}}}\sum_{\boldsymbol{k}}\frac{\varepsilon^2_{\boldsymbol{k}}}{r_U U^2}\right).$$

Thus $\chi_0(\boldsymbol{q};0)$ is indeed larger at $\boldsymbol{q} = \boldsymbol{q}_C$ than at $\boldsymbol{q} = \mathbf{0}$; it is however weakly temperature dependent and does not exhibit Curie-Weiss instabilities. The calculation presented above can be generalized to any $\boldsymbol{q}$ vector [11], obtaining the expression

$$\chi_0(\boldsymbol{q};0) \sim (g\mu_B)^2\frac{1}{4\sqrt{r_U}U}\left(1 - \frac{1}{2}\frac{J_{\mathbf{0}}}{\sqrt{r_U}U} - \frac{1}{4}\frac{J_{\boldsymbol{q}}}{\sqrt{r_U}U}\right), \tag{32}$$

where $J_{\boldsymbol{q}} = J\big(\cos q_x + \cos q_y\big)$, and the super-exchange coupling is $J = 4t^2/U$. To make progress we now need the local vertex. This requires, as we have seen, the solution of the self-consistent quantum-impurity model via the quantum-impurity solver. Here, for the purpose of illustrating how the approach works, we approximate the local susceptibility with the atomic susceptibility in the large βU limit. Furthermore we work with the susceptibilities obtained *after* the Matsubara sums have been performed. Thus

$$\chi^0_{zz}(0) \sim (g\mu_B)^2\frac{1}{4\sqrt{r_U}U}, \qquad \chi_{zz}(0) \sim \frac{1}{4k_BT}.$$

The local vertex is then approximately given by

$$\Gamma \sim \frac{1}{\chi^0_{zz}(0)} - \frac{1}{\chi_{zz}(0)} \sim \frac{1}{(g\mu_B)^2}\left[4\sqrt{r_U}U\left(1 + \frac{1}{2}\frac{J_{\mathbf{0}}}{\sqrt{r_U}U}\right) - 4k_BT\right].$$

The last step consists in solving the Bethe-Salpeter equation

$$\chi_{zz}(\boldsymbol{q};0) = \frac{1}{(\chi^0_{zz}(\boldsymbol{q};0))^{-1} - \Gamma} \sim \frac{(g\mu_B)^2}{4}\frac{1}{k_BT + J_{\boldsymbol{q}}/4} = \frac{(g\mu_B)^2}{4k_B}\,\frac{1}{T - T_{\boldsymbol{q}}}.$$

This shows that including the local vertex correction we recover the Curie-Weiss behavior, as expected for a system described by local spins coupled by a Heisenberg-like exchange; we also correctly find the antiferromagnetic instability, since $\boldsymbol{q}_C$ is the vector for which the critical temperature $T_{\boldsymbol{q}}$ is the largest. In conclusion, we have seen that $\Gamma(i\omega_m)$ is essential to properly describe the magnetic response function of strongly-correlated systems. This can be seen in Fig. 12 for the Mott insulator $VOMoO_4$. In the figure we can compare the very weak linear magnetic response $\chi_0(\boldsymbol{q};0)$ (upper panels) with the LDA+DMFT result $\chi(\boldsymbol{q};0)$ (lower panels). The latter is not only strongly enhanced with respect to $\chi_0(\boldsymbol{q};0)$, but also exhibits the expected Curie-Weiss like behavior, as can be seen in Fig. 15 for $\boldsymbol{q} = \mathbf{0}$.

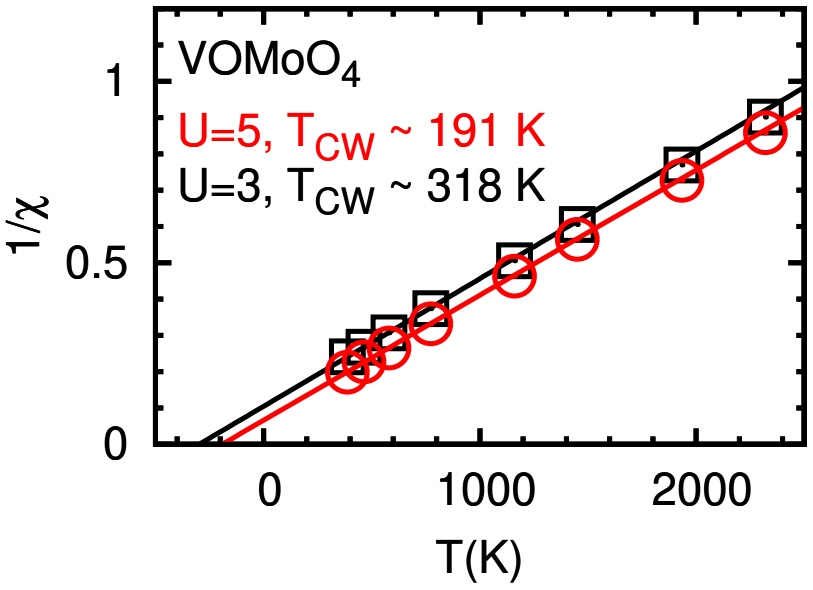

Fig. 15: *$VOMoO_4$: The Curie-Weiss behavior of the uniform magnetic susceptibility at half filling, obtained with the LDA+DMFT approach. Rearranged from Ref. [11].*

4 Conclusion

The LDA+DMFT approach and its extension has proved very successful for describing correlated materials. It has shown us that materials details do matter, contrarily to what often was assumed in the past; for example a crystal field much smaller than the bandwidth can favor the Mott metal-insulator transition [18]. The method is becoming progressively more and more versatile. It is now possible, e.g., to study multi-orbital Hubbard-like models including the full Coulomb vertex and the spin-orbit interaction. Successful extension schemes, e.g., cluster methods, account, at least in part, for the $\boldsymbol{q}$-dependence of the self-energy. In this lecture, we have seen how to use the LDA+DMFT approach to calculate not only Green and spectral functions but also linear-response functions. In the scheme presented, the local susceptibility is obtained via the quantum-impurity solver at the end of the self-consistency loop; the $\boldsymbol{q}$-dependent susceptibility is, instead, calculated solving in addition the Bethe-Salpeter equation in the local-vertex approximation. As representative case we have studied the magnetic susceptibility of the one-band Hubbard model at half filling. The extension of the LDA+DMFT approach to the calculation of generalized susceptibilities makes it possible to put the method and the approximations adopted to more stringent tests. This is key for further advancing the theoretical tools for the description of strong correlation effects in real materials.

Appendix

A Eigenstates of two-site models

A.1 Hubbard dimer

The Hamiltonian of the Hubbard dimer is given by

$$\hat{H} = \varepsilon_d \sum_{\sigma} \sum_{i=1,2} \hat{n}_{i\sigma} - t \sum_{\sigma} \left(c^{\dagger}_{1\sigma} c_{2\sigma} + c^{\dagger}_{2\sigma} c_{1\sigma} \right) + U \sum_{i=1,2} \hat{n}_{i\uparrow} \hat{n}_{i\downarrow}.$$

It commutes with the number of electron operator $\hat{N}$, with the total spin $\hat{S}$ and with $\hat{S}_z$. Thus we can express the many-body states in the atomic limit as

$\lvert N, S, S_z \rangle$			N	S	$E(N,S)$
$\lvert 0,0,0 \rangle$	$=$	$\lvert 0 \rangle$	0	0	0
$\lvert 1,1/2,\sigma \rangle_1$	$=$	$c^{\dagger}_{1\sigma} \lvert 0 \rangle$	1	$1/2$	ε_d
$\lvert 1,1/2,\sigma \rangle_2$	$=$	$c^{\dagger}_{2\sigma} \lvert 0 \rangle$	1	$1/2$	ε_d
$\lvert 2,1,1 \rangle$	$=$	$c^{\dagger}_{2\uparrow} c^{\dagger}_{1\uparrow} \lvert 0 \rangle$	2	1	$2\varepsilon_d$
$\lvert 2,1,-1 \rangle$	$=$	$c^{\dagger}_{2\downarrow} c^{\dagger}_{1\downarrow} \lvert 0 \rangle$	2	1	$2\varepsilon_d$
$\lvert 2,1,0 \rangle$	$=$	$\frac{1}{\sqrt{2}} \left(c^{\dagger}_{1\uparrow} c^{\dagger}_{2\downarrow} + c^{\dagger}_{1\downarrow} c^{\dagger}_{2\uparrow} \right) \lvert 0 \rangle$	2	1	$2\varepsilon_d$
$\lvert 2,0,0 \rangle_0$	$=$	$\frac{1}{\sqrt{2}} \left(c^{\dagger}_{1\uparrow} c^{\dagger}_{2\downarrow} - c^{\dagger}_{1\downarrow} c^{\dagger}_{2\uparrow} \right) \lvert 0 \rangle$	2	0	$2\varepsilon_d$
$\lvert 2,0,0 \rangle_1$	$=$	$c^{\dagger}_{1\uparrow} c^{\dagger}_{1\downarrow} \lvert 0 \rangle$	2	0	$2\varepsilon_d + U$
$\lvert 2,0,0 \rangle_2$	$=$	$c^{\dagger}_{2\uparrow} c^{\dagger}_{2\downarrow} \lvert 0 \rangle$	2	0	$2\varepsilon_d + U$
$\lvert 3,1/2,\sigma \rangle_1$	$=$	$c^{\dagger}_{1\sigma} c^{\dagger}_{2\uparrow} c^{\dagger}_{2\downarrow} \lvert 0 \rangle$	3	$1/2$	$3\varepsilon_d + U$
$\lvert 3,1/2,\sigma \rangle_2$	$=$	$c^{\dagger}_{2\sigma} c^{\dagger}_{1\uparrow} c^{\dagger}_{1\downarrow} \lvert 0 \rangle$	3	$1/2$	$3\varepsilon_d + U$
$\lvert 4,0,0 \rangle$	$=$	$c^{\dagger}_{1\uparrow} c^{\dagger}_{1\downarrow} c^{\dagger}_{2\uparrow} c^{\dagger}_{2\downarrow} \lvert 0 \rangle$	4	0	$4\varepsilon_d + 2U$

Let us order the $N = 1$ states as in the table above, first the spin up and then spin down block. For finite t the Hamiltonian matrix for $N = 1$ electrons takes then the form

$$\hat{H}_1 = \begin{pmatrix} \varepsilon_d & -t & 0 & 0 \\ -t & \varepsilon_d & 0 & 0 \\ 0 & 0 & \varepsilon_d & -t \\ 0 & 0 & -t & \varepsilon_d \end{pmatrix}.$$

This matrix can be easily diagonalized and yields the *bonding* $(-)$ and *antibonding* $(+)$ states

$\|1,S,S_z\rangle_\alpha$	$E_\alpha(1,S)$	$d_\alpha(1,S)$
$\|1,1/2,\sigma\rangle_+ = \frac{1}{\sqrt{2}}\big(\|1,1/2,\sigma\rangle_1 - \|1,1/2,\sigma\rangle_2\big)$	$\varepsilon_d + t$	2
$\|1,1/2,\sigma\rangle_- = \frac{1}{\sqrt{2}}\big(\|1,1/2,\sigma\rangle_1 + \|1,1/2,\sigma\rangle_2\big)$	$\varepsilon_d - t$	2

where $d_\alpha(N)$ is the spin degeneracy of the α manifold.
For $N = 2$ electrons (half filling), the hopping integrals only couple the three $S = 0$ states, and therefore the Hamiltonian matrix is given by

$$\hat{H}_2 = \begin{pmatrix} 2\varepsilon_d & 0 & 0 & 0 & 0 & 0 \\ 0 & 2\varepsilon_d & 0 & 0 & 0 & 0 \\ 0 & 0 & 2\varepsilon_d & 0 & 0 & 0 \\ 0 & 0 & 0 & 2\varepsilon_d & -\sqrt{2}t & -\sqrt{2}t \\ 0 & 0 & 0 & -\sqrt{2}t & 2\varepsilon_d + U & 0 \\ 0 & 0 & 0 & -\sqrt{2}t & 0 & 2\varepsilon_d + U \end{pmatrix}.$$

The eigenvalues and the corresponding eigenvectors are

$\|2,S,S_z\rangle_\alpha$	$E_\alpha(2,S)$	$d_\alpha(2,S)$
$\|2,0,0\rangle_+ = a_1\|2,0,0\rangle_0 - \frac{a_2}{\sqrt{2}}\big(\|2,0,0\rangle_1 + \|2,0,0\rangle_2\big)$	$2\varepsilon_d + \frac{1}{2}\left(U + \Delta(t,U)\right)$	1
$\|2,0,0\rangle_o = \frac{1}{\sqrt{2}}\big(\|2,0,0\rangle_1 - \|2,0,0\rangle_2\big)$	$2\varepsilon_d + U$	1
$\|2,1,m\rangle_o = \|2,1,m\rangle$	$2\varepsilon_d$	3
$\|2,0,0\rangle_- = a_2\|2,0,0\rangle_0 + \frac{a_1}{\sqrt{2}}\big(\|2,0,0\rangle_1 + \|2,0,0\rangle_2\big)$	$2\varepsilon_d + \frac{1}{2}\left(U - \Delta(t,U)\right)$	1

where

$$\Delta(t,U) = \sqrt{U^2 + 16t^2},$$

and

$$a_1^2 = a_1^2(t,U) = \frac{1}{\Delta(t,U)}\frac{\Delta(t,U) - U}{2} \qquad a_2^2 = a_2^2(t,U) = \frac{4t^2}{\Delta(t,U)}\frac{2}{(\Delta(t,U) - U)},$$

so that $a_1 a_2 = 2t/\Delta(t,U)$. For $U = 0$ we have $a_1 = a_2 = 1/\sqrt{2}$, and the two states $|2,0,0\rangle_-$ and $|2,0,0\rangle_+$ become, respectively, the state with two electrons in the bonding orbital and the state with two electrons in the antibonding orbital; they have energy $E_\pm(2,0) = 2\varepsilon_d \pm 2t$; the remaining states have energy $2\varepsilon_d$ and are non-bonding. For $t > 0$, the ground state is unique and it is always the singlet $|2,0,0\rangle_-$; in the large U limit its energy is

$$E_-(2,0) \sim 2\varepsilon_d - 4t^2/U.$$

In this limit the energy difference between the first excited state, a triplet state, and the singlet ground state is thus equal to the Heisenberg antiferromagnetic coupling

$$E_o(2,1) - E_-(2,0) \sim 4t^2/U = \Gamma.$$

Finally, for $N = 3$ electrons, eigenstates and eigenvectors are

$\lvert 3,S,S_z\rangle_\alpha$		$E_\alpha(3)$	$d_\alpha(3,S)$
$\lvert 3,1/2,\sigma\rangle_+$	$= \frac{1}{\sqrt{2}}\big(\lvert 1,1/2,\sigma\rangle_1 + \lvert 1,1/2,\sigma\rangle_2\big)$	$3\varepsilon_d + U + t$	2
$\lvert 3,1/2,\sigma\rangle_-$	$= \frac{1}{\sqrt{2}}\big(\lvert 1,1/2,\sigma\rangle_1 - \lvert 1,1/2,\sigma\rangle_2\big)$	$3\varepsilon_d + U - t$	2

If we exchange holes and electrons, the $N = 3$ case is identical to the $N = 1$ electron case. This is due to the particle-hole symmetry of the model.

A.2 Anderson molecule

The Hamiltonian of the Anderson molecule is given by

$$\hat{H} = \varepsilon_s \sum_\sigma \hat{n}_{2\sigma} - t \sum_\sigma \left(c^\dagger_{1\sigma} c_{2\sigma} + c^\dagger_{2\sigma} c_{1\sigma}\right) + \varepsilon_d \sum_\sigma \hat{n}_{1\sigma} + U \hat{n}_{1\uparrow}\hat{n}_{1\downarrow}.$$

In the atomic limit, its eigenstates states can be classified as

$\lvert N,S,S_z\rangle$			N	S	$E(N,S)$
$\lvert 0,0,0\rangle$	$=$	$\lvert 0\rangle$	0	0	0
$\lvert 1,1/2,\sigma\rangle_1$	$=$	$c^\dagger_{1\sigma}\lvert 0\rangle$	1	1/2	ε_d
$\lvert 1,1/2,\sigma\rangle_2$	$=$	$c^\dagger_{2\sigma}\lvert 0\rangle$	1	1/2	ε_s
$\lvert 2,1,1\rangle$	$=$	$c^\dagger_{2\uparrow}c^\dagger_{1\uparrow}\lvert 0\rangle$	2	1	$\varepsilon_d + \varepsilon_s$
$\lvert 2,1,-1\rangle$	$=$	$c^\dagger_{2\downarrow}c^\dagger_{1\downarrow}\lvert 0\rangle$	2	1	$\varepsilon_d + \varepsilon_s$
$\lvert 2,1,0\rangle$	$=$	$\frac{1}{\sqrt{2}}\left(c^\dagger_{1\uparrow}c^\dagger_{2\downarrow} + c^\dagger_{1\downarrow}c^\dagger_{2\uparrow}\right)\lvert 0\rangle$	2	1	$\varepsilon_d + \varepsilon_s$
$\lvert 2,0,0\rangle_0$	$=$	$\frac{1}{\sqrt{2}}\left(c^\dagger_{1\uparrow}c^\dagger_{2\downarrow} - c^\dagger_{1\downarrow}c^\dagger_{2\uparrow}\right)\lvert 0\rangle$	2	0	$\varepsilon_d + \varepsilon_s$
$\lvert 2,0,0\rangle_1$	$=$	$c^\dagger_{1\uparrow}c^\dagger_{1\downarrow}\lvert 0\rangle$	2	0	$2\varepsilon_d + U$
$\lvert 2,0,0\rangle_2$	$=$	$c^\dagger_{2\uparrow}c^\dagger_{2\downarrow}\lvert 0\rangle$	2	0	$2\varepsilon_s$
$\lvert 3,1/2,\sigma\rangle_1$	$=$	$c^\dagger_{1\sigma}c^\dagger_{2\uparrow}c^\dagger_{2\downarrow}\lvert 0\rangle$	3	1/2	$\varepsilon_d + 2\varepsilon_s$
$\lvert 3,1/2,\sigma\rangle_2$	$=$	$c^\dagger_{2\sigma}c^\dagger_{1\uparrow}c^\dagger_{1\downarrow}\lvert 0\rangle$	3	1/2	$2\varepsilon_d + \varepsilon_s + U$
$\lvert 4,0,0\rangle$	$=$	$c^\dagger_{1\uparrow}c^\dagger_{1\downarrow}c^\dagger_{2\uparrow}c^\dagger_{2\downarrow}\lvert 0\rangle$	4	0	$2\varepsilon_d + 2\varepsilon_s + U$

For $N = 1$ electrons the Hamiltonian can be written in the matrix form

$$\hat{H}_1 = \begin{pmatrix} \varepsilon_d & -t & 0 & 0 \\ -t & \varepsilon_s & 0 & 0 \\ 0 & 0 & \varepsilon_d & -t \\ 0 & 0 & -t & \varepsilon_s \end{pmatrix}.$$

The eigenstates are thus

$\|1, S, S_z\rangle_\alpha$	$E_\alpha(1, S)$	$d_\alpha(1, S)$
$\|1, 1/2, \sigma\rangle_+ = \alpha_1 \|1, 1/2, \sigma\rangle_1 - \alpha_2 \|1, 1/2, \sigma\rangle_2$	$\frac{1}{2}\big(\varepsilon_d + \varepsilon_s + \sqrt{(\varepsilon_d - \varepsilon_s)^2 + 4t^2}\big)$	2
$\|1, 1/2, \sigma\rangle_- = \alpha_2 \|1, 1/2, \sigma\rangle_1 + \alpha_1 \|1, 1/2, \sigma\rangle_2$	$\frac{1}{2}\big(\varepsilon_d + \varepsilon_s - \sqrt{(\varepsilon_d - \varepsilon_s)^2 + 4t^2}\big)$	2

where $d_\alpha(N)$ is the spin degeneracy of the α manifold. For $\varepsilon_s = \varepsilon_d + U/2$ the eigenvalues are

$$E_\pm(1, S) = \varepsilon_d + \frac{1}{4}\big(U \pm \Delta(t, U)\big),$$

while the coefficients are $\alpha_1 = a_1(t, U)$ and $\alpha_2 = a_2(t, U)$.
For N=2 electrons, the hopping integrals only couple the S=0 states. The Hamiltonian is

$$\hat{H}_2 = \begin{pmatrix} \varepsilon_d{+}\varepsilon_s & 0 & 0 & 0 & 0 & 0 \\ 0 & \varepsilon_d{+}\varepsilon_s & 0 & 0 & 0 & 0 \\ 0 & 0 & \varepsilon_d{+}\varepsilon_s & 0 & 0 & 0 \\ 0 & 0 & 0 & \varepsilon_d{+}\varepsilon_s & -\sqrt{2}t & -\sqrt{2}t \\ 0 & 0 & 0 & -\sqrt{2}t & 2\varepsilon_d{+}U & 0 \\ 0 & 0 & 0 & -\sqrt{2}t & 0 & 2\varepsilon_s \end{pmatrix}$$

For $\varepsilon_s = \varepsilon_d + U/2$ the eigenvalues and the corresponding eigenvectors are

$\|2, S, S_z\rangle_\alpha$	$E_\alpha(2, S)$	$d_\alpha(2, S)$
$\|2, 0, 0\rangle_+ = b_1 \|2, 0, 0\rangle_0 - \frac{b_2}{\sqrt{2}}\big(\|2, 0, 0\rangle_1 + \|2, 0, 0\rangle_2\big)$	$2\varepsilon_d + \frac{U}{2} + \frac{1}{4}\big(U + 2\Delta(t, \frac{U}{2})\big)$	1
$\|2, 0, 0\rangle_o = \frac{1}{\sqrt{2}}\big(\|2, 0, 0\rangle_1 - \|2, 0, 0\rangle_2\big)$	$2\varepsilon_d + U$	1
$\|2, 1, m\rangle_o = \|2, 1, m\rangle$	$2\varepsilon_d + \frac{U}{2}$	3
$\|2, 0, 0\rangle_- = b_2 \|2, 0, 0\rangle_0 + \frac{b_1}{\sqrt{2}}\big(\|2, 0, 0\rangle_1 + \|2, 0, 0\rangle_2\big)$	$2\varepsilon_d + \frac{U}{2} + \frac{1}{4}\big(U - 2\Delta(t, \frac{U}{2})\big)$	1

where $b_1 = a_1(t, U/2)$ and $b_2 = a_2(t, U/2)$. These states have the same form as in the case of the Hubbard dimer; the ground state energy and the weight of doubly occupied states in $|2, 0, 0\rangle_-$ differ, however. Finally, for $N = 3$ electrons, the eigenstates are

$\|3, S, S_z\rangle_\alpha$	$E_\alpha(3, S)$	$d_\alpha(3, S)$
$\|3, 1/2, \sigma\rangle_+ = \alpha_2 \|1, 1/2, \sigma\rangle_1 + \alpha_1 \|1, 1/2, \sigma\rangle_2$	$3\varepsilon_d + U + \frac{1}{4}\big(U + \Delta(t, U)\big)$	2
$\|3, 1/2, \sigma\rangle_- = \alpha_1 \|1, 1/2, \sigma\rangle_1 - \alpha_2 \|1, 1/2, \sigma\rangle_2$	$3\varepsilon_d + U + \frac{1}{4}\big(U - \Delta(t, U)\big)$	2

B Lehmann representation of the local Green function

For a single-orbital model, the local Matsubara Green function for a given site i is defined as

$$G^{\sigma}_{i,i}(i\nu_n) = -\int_0^{\beta} d\tau e^{i\nu_n\tau}\big\langle \mathcal{T} c_{i\sigma}(\tau)c^{\dagger}_{i\sigma}(0)\big\rangle,$$

where $\mathcal{T}$ is the time-ordering operator, $\beta = 1/k_BT$, and ν_n a fermionic Matsubara frequency. Let us assume we know all eigenstates $|N_l\rangle$ and their energy $E_l(N)$, for arbitrary number of electrons N. Thus, formally

$$G^{\sigma}_{i,i}(i\nu_n) = -\frac{1}{Z}\sum_{Nl}\int_0^{\beta} d\tau e^{i\nu_n\tau}e^{-\Delta E_l(N)\beta}\big\langle N_l\big|c_{i\sigma}(\tau)c^{\dagger}_{i\sigma}(0)\big|N_l\big\rangle,$$

where $Z = \sum_{Nl} e^{-\Delta E_l(N)\beta}$ is the partition function, $\Delta E_l(N) = E_l(N) - \mu N$ with μ the chemical potential, and $c^{\dagger}_{i\sigma}(0) = c^{\dagger}_{i\sigma}$. We now insert a complete set of states, obtaining

$$\begin{aligned} G^{\sigma}_{i,i}(i\nu_n) &= -\frac{1}{Z}\sum_{ll'NN'}\int_0^{\beta} d\tau e^{i\nu_n\tau}e^{-\Delta E_l(N)\beta}\big\langle N_l\big|c_{i\sigma}(\tau)|N'_{l'}\big\rangle\big\langle N'_{l'}\big|c^{\dagger}_{i\sigma}\big|N_l\big\rangle \\ &= -\frac{1}{Z}\sum_{ll'NN'}\int_0^{\beta} d\tau e^{-\Delta E_l(N)\beta}e^{(i\nu_n+\Delta E_l(N)-\Delta E_{l'}(N'))\tau}\big|\langle N'_{l'}|c^{\dagger}_{i\sigma}|N_l\rangle\big|^2 \\ &= \frac{1}{Z}\sum_{ll'NN'}\frac{e^{-\Delta E_{l'}(N')\beta}+e^{-\Delta E_l(N)\beta}}{i\nu_n+\Delta E_l(N)-\Delta E_{l'}(N')}\big|\langle N'_{l'}|c^{\dagger}_{i\sigma}|N_l\rangle\big|^2. \end{aligned}$$

Due to the weight $\big|\langle N'_{l'}|c^{\dagger}_{i\sigma}(0)|N_l\rangle\big|^2$ only the terms for which $N' = N+1$ contribute. Thus, after exchanging the labels $l'N' \leftrightarrow lN$ in the first addend, we obtain the Lehmann representation

$$G^{\sigma}_{i,i}(i\nu_n)=\sum_{ll'N}\frac{e^{-\beta\Delta E_l(N)}}{Z}\left(\frac{\big|\langle(N-1)_{l'}|c_{i\sigma}|N_l\rangle\big|^2}{i\nu_n-\Delta E_l(N)+\Delta E_{l'}(N-1)}+\frac{\big|\langle(N+1)_{l'}|c^{\dagger}_{i\sigma}|N_l\rangle\big|^2}{i\nu_n-\Delta E_{l'}(N+1)+\Delta E_l(N)}\right).$$

Let us consider as example the atomic limit of the Hubbard model at half filling. In this case all sites are decoupled; there are four eigenstates per site, the vacuum $|0\rangle$, with $\Delta E(0) = 0$, the doublet $|1_\sigma\rangle = c^{\dagger}_{i\sigma}|0\rangle$, with $\Delta E_\sigma(1) = -U/2$, and the doubly-occupied singlet $|2\rangle = c^{\dagger}_{i\uparrow}c^{\dagger}_{i\downarrow}|0\rangle$, with $\Delta E(2) = 0$. Furthermore, $Z = 2(1 + e^{\beta U/2})$ and

$$\big|\langle(N-1)_{l'}|c_{i\sigma}|N_l\rangle\big|^2=\begin{cases}1 & \text{if } |N_l\rangle=|2\rangle\vee|1_\sigma\rangle\\ 0 & \text{otherwise}\end{cases}\qquad \big|\langle(N+1)_{l'}|c^{\dagger}_{i\sigma}|N_l\rangle\big|^2=\begin{cases}1 & \text{if } |N_l\rangle=|0\rangle\vee|1_{-\sigma}\rangle\\ 0 & \text{otherwise}\end{cases}$$

Thus, after summing up the four non-zero contributions, we find

$$G^{\sigma}_{i,i}(\nu_n) = \frac{1}{2}\left(\frac{1}{i\nu_n+U/2}+\frac{1}{i\nu_n-U/2}\right).$$

C Atomic magnetic susceptibility

Let us consider an idealized single-level atom described by the Hamiltonian

$$\hat{H} = \varepsilon_d\big(\hat{n}_\uparrow + \hat{n}_\downarrow\big) + U n_\uparrow n_\downarrow.$$

The eigenstates of this system, $|\Psi_i^N\rangle$, as well as their expectation values at half filling are

$\lvert\Psi_i^N\rangle$	N	$\Delta E_i = \big\langle\Psi_i^N\big\lvert\hat{H}-\mu\hat{N}\big\rvert\Psi_i^N\big\rangle$
$\lvert 0\rangle$	0	0
$c_\sigma^\dagger\lvert 0\rangle$	1	$-\frac{U}{2}$
$c_\uparrow^\dagger c_\downarrow^\dagger\lvert 0\rangle$	2	0

The magnetic susceptibility in Matsubara space is given by

$$\Big[\chi_{zz}(i\omega_m)\Big]_{nn'} = \beta\frac{1}{4}(g\mu_B)^2\sum_P \mathrm{sign}(P) f_P$$

$$f_P(i\omega_{P_1}, i\omega_{P_2}, i\omega_{P_3}) = \int_0^\beta d\tau_{14}\int_0^{\tau_{14}} d\tau_{24}\int_0^{\tau_{24}} d\tau_{34}\; e^{i\omega_{P_1}\tau_{14}+i\omega_{P_2}\tau_{24}+i\omega_{P_3}\tau_{34}} f_P(\tau_{14},\tau_{24},\tau_{34})$$

where $P = A, B, \ldots$ are the six possible permutations of the indices (123) and

$$\begin{aligned} f_P(\tau_{14},\tau_{24},\tau_{34}) &= \frac{1}{Z}\sum_{\sigma\sigma'}\sigma\sigma'\mathrm{Tr}\; e^{-\beta(\hat{H}-\mu\hat{N})}\Big[\hat{o}_{P_1}(\tau_{14})\hat{o}_{P_2}(\tau_{24})\hat{o}_{P_3}(\tau_{34})c_{\sigma'}^\dagger\Big] \\ &= \frac{1}{Z}\sum_{\sigma\sigma'}\sigma\sigma'\sum_{ijkl} e^{-\beta\Delta E_i}\langle i|\hat{o}_{P_1}|j\rangle\langle j|\hat{o}_{P_2}|k\rangle\langle k|\hat{o}_{P_3}|l\rangle\langle l|c_{\sigma'}^\dagger|i\rangle \\ &\quad\times\left[e^{\Delta E_{ij}\tau_{14}+\Delta E_{jk}\tau_{24}+\Delta E_{kl}\tau_{34}}\right], \end{aligned}$$

where $\Delta E_{ij} = \Delta E_i - \Delta E_j$. For the identity permutation the operators are $\hat{o}_{P_1} = c_\sigma$, $\hat{o}_{P_2} = c_\sigma^\dagger$, and $\hat{o}_{P_3} = c_{\sigma'}$ and the frequencies are $\omega_1 = \nu_n$, $\omega_2 = -\omega_m - \nu_n$, $\omega_3 = \omega_m + \nu_{n'}$. This expression can be used to calculate the magnetic susceptibility of any one-band system whose eigenvalues and eigenvectors are known, e.g., via exact diagonalization. In the case of our idealized atom

$$f_E(\tau_{14},\tau_{24},\tau_{34}) = \frac{1}{(1+e^{\beta U/2})}\; e^{\beta U/2}\; e^{-(\tau_{12}+\tau_{34})U/2} = \frac{1}{(1+e^{\beta U/2})}\; g_E(\tau_{14},\tau_{24},\tau_{34}).$$

The frequencies and functions $f_P(\tau_{14},\tau_{24},\tau_{34})$ for all permutations are given in the table below

	ω_{P_1}	ω_{P_2}	ω_{P_3}	$g_P(\tau_{14},\tau_{24},\tau_{34})$	$\mathrm{sign}(P)$
$E(123)$	ν_n	$-\omega_m-\nu_n$	$\omega_m+\nu_{n'}$	$e^{\beta U/2}\, e^{-(\tau_{12}+\tau_{34})U/2}$	$+$
$A(231)$	$-\omega_m-\nu_n$	$\omega_m+\nu_{n'}$	ν_n	$e^{\beta U/2}\, e^{-(\tau_{12}+\tau_{34})U/2}$	$+$
$B(312)$	$\omega_m+\nu_{n'}$	ν_n	$-\omega_m-\nu_n$	$-e^{+(\tau_{12}+\tau_{34})U/2}$	$+$
$C(213)$	$-\omega_m-\nu_n$	ν_n	$\omega_m+\nu_{n'}$	$-e^{\beta U/2}e^{-(\tau_{12}+\tau_{34})U/2}$	$-$
$D(132)$	ν_n	$\omega_m+\nu_{n'}$	$-\omega_m-\nu_n$	$e^{+(\tau_{12}+\tau_{34})U/2}$	$-$
$F(321)$	$\omega_m+\nu_{n'}$	$-\omega_m-\nu_n$	ν_n	$e^{+(\tau_{12}+\tau_{34})U/2}$	$-$

The missing ingredient is the integral

$$
\begin{aligned}
I_P(x,-x,x;i\omega_{P_1},i\omega_{P_2},i\omega_{P_3}) &= \int_0^\beta d\tau_{14}\int_0^{\tau_{14}} d\tau_{24}\int_0^{\tau_{24}} d\tau_{34}\, e^{i\omega_{P_1}\tau_{14}+i\omega_{P_2}\tau_{24}+i\omega_{P_3}\tau_{34}} e^{x(\tau_{14}-\tau_{24}+\tau_{34})} \\
&= +\int_0^\beta d\tau_{14}\int_0^{\tau_{14}} d\tau\int_0^{\tau_{14}-\tau} d\tau'\, e^{(i\omega_{P_1}+i\omega_{P_2}+i\omega_{P_3}+x)\tau_{14}-i(\omega_{P_2}+\omega_{P_3})\tau} e^{-(i\omega_{P_3}+x)\tau'} \\
&= +\frac{1}{i\omega_{P_3}+x}\frac{1}{-i\omega_{P_2}+x}\left[\frac{1}{i\omega_{P_1}+x}\,\frac{1}{n(x)}+\beta\delta_{\omega_{P_1}+\omega_{P_2}}\right] \\
&\quad +\frac{1}{i\omega_{P_3}+x}\frac{1-\delta_{\omega_{P_2}+\omega_{P_3}}}{i(\omega_{P_2}+\omega_{P_3})}\left[\frac{1}{i\omega_{P_1}+x}-\frac{1}{i(\omega_{P_1}+\omega_{P_2}+\omega_{P_3})+x}\right]\frac{1}{n(x)} \\
&\quad +\delta_{\omega_{P_2}+\omega_{P_3}}\frac{1}{i\omega_{P_3}+x}\left\{\left[\frac{1}{(i\omega_{P_1}+x)}\right]^2\frac{1}{n(x)}-\beta\left[\frac{1}{(i\omega_{P_1}+x)}\right]\frac{1-n(x)}{n(x)}\right\}.
\end{aligned}
$$

where $x = \pm U/2$, depending on the permutation. Summing up all terms we obtain the final expression for $\omega_m = 0$. Setting $y = U/2$ we have in total [11]

$$
\begin{aligned}
\sum_{\sigma\sigma'}\sigma\sigma'\,\chi^{n,n'}_{i\sigma\sigma,i\sigma'\sigma'}(0) =& M_{n'}\frac{dM_n}{dy}+M_n\frac{dM_{n'}}{dy}-\beta n(y)\left[\delta_{n,n'}+\delta_{n,-n'}\right]\frac{dM_n}{dy}+\beta n(-y)M_nM_{n'} \\
&-\frac{1}{y}\left\{M_{n'}-\beta\left[n(y)\delta_{n,-n'}-n(-y)\delta_{n,n'}\right]\right\}M_n
\end{aligned}
\tag{33}
$$

where

$$
M_n = \frac{1}{i\nu_n - y}-\frac{1}{i\nu_n+y}. \tag{34}
$$

The finite frequency term (not given here) vanishes once we sum over n, n'.

References

[1] W. Metzner and D. Vollhardt, Phys. Rev. Lett. **62**, 324 (1989)

[2] E. Müller-Hartmann, Z. Phys. B **74**, 507 (1989); Z. Phys. B **76**, 211 (1989);
Int. J. Mod. Phys. B **3**, 2169 (1989)

[3] A. Georges and G. Kotliar, Phys. Rev. B **45**, 6479 (1992)

[4] M. Jarrell, Phys. Rev. Lett. **69**, 168 (1992)

[5] E. Pavarini, E. Koch, D. Vollhardt, A. Lichtenstein (Eds.):
The LDA+DMFT approach to strongly-correlated materials,
Reihe Modeling and Simulation, Vol. 1 (Forschungszentrum Jülich, 2011)
`http://www.cond-mat.de/events/correl11`

[6] E. Pavarini, E. Koch, A. Lichtenstein, D. Vollhardt (Eds.):
DMFT at 25: Infinite Dimensions,
Reihe Modeling and Simulation, Vol. 4 (Forschungszentrum Jülich, 2014)
`http://www.cond-mat.de/events/correl14`

[7] E. Pavarini, E. Koch, A. Lichtenstein, D. Vollhardt (Eds.):
DMFT: From Infinite Dimensions to Real Materials,
Reihe Modeling and Simulation, Vol. 8 (Forschungszentrum Jülich, 2018)
`http://www.cond-mat.de/events/correl18`

[8] E. Koch, G. Sangiovanni, and O. Gunnarsson, Phys. Rev. B **78**, 115102 (2008)

[9] E. Gull, A.J. Millis, A.I. Lichtenstein, A.N. Rubtsov, M. Troyer, and P. Werner,
Rev. Mod. Phys. **83**, 349 (2011)

[10] A. Flesch, E. Gorelov, E. Koch, E. Pavarini, Phys. Rev. B **87**, 195141 (2013)

[11] A. Kiani and E. Pavarini, Phys. Rev. B **94**, 075112 (2016)

[12] E. Pavarini, A. Yamasaki, J. Nuss, and O.K. Andersen, New. J. Phys **7**, 188 (2005)

[13] N. Marzari, A.A. Mostofi, J.R. Yates, I. Souza, and D. Vanderbilt,
Rev. Mod. Phys. **84**, 1419 (2012)

[14] V. Slatić and B. Horvatić, Sol. Stat. Comm. **75**, 263 (1990)

[15] L. Boehnke, H. Hafermann, M. Ferrero, F. Lechermann and O. Parcollet,
Phys. Rev. B **84**, 075145 (2011)

[16] J. Musshoff, G. Zhang, E. Koch, and E. Pavarini, Phys. Rev. B **100**, 045116 (2019)

[17] A. Georges, G. Kotliar, W. Krauth and M.J. Rozenberg, Rev. Mod. Phys. **68**, 13 (1996)

[18] E. Pavarini, S. Biermann, A. Poteryaev, A.I. Lichtenstein, A. Georges, and O.K. Andersen,
Phys. Rev. Lett. **92**, 176403 (2004)